



Ward identity determination of Z_S/Z_P for $N_f = 3$ lattice QCD in a Schrödinger functional setup

ALPHA Collaboration

Jochen Heitger¹ , Fabian Joswig^{1,a}, Anastassios Vladikas²

¹ Institut für Theoretische Physik, Westfälische Wilhelms-Universität Münster, Wilhelm-Klemm-Straße 9, 48149 Münster, Germany

² “Rome Tor Vergata” Division, c/o Dipartimento di Fisica, INFN, Via della Ricerca Scientifica 1, 00133 Rome, Italy

Received: 12 May 2020 / Accepted: 21 July 2020 / Published online: 24 August 2020
© The Author(s) 2020

Abstract We derive chiral Ward identities for lattice QCD with Wilson quarks and $N_f \geq 3$ flavours, on small lattices with Schrödinger functional boundary conditions and vanishingly small quark masses. These identities relate the axial variation of the non-singlet pseudoscalar density to the scalar one, thus enabling the non-perturbative determination of the scale-independent ratio Z_S/Z_P of the renormalisation parameters of these operators. We obtain results for $N_f = 3$ QCD with tree-level Symanzik-improved gluons and Wilson-Clover quarks, for bare gauge couplings which cover the typical range of large-volume $N_f = 2 + 1$ simulations with Wilson fermions at lattice spacings below 0.1 fm. The precision of our results varies from 0.3 to 1%, except for the coarsest lattice, where it is 2%. We discuss how the Z_S/Z_P ratio can be used in the non-perturbative calculations of $O(a)$ improved renormalised quark masses.

Contents

1 Introduction	1
2 Chiral Ward identities for Z_S/Z_P	3
2.1 Formal chiral Ward identities in the continuum	3
2.2 Lattice Ward identities with Schrödinger functional boundary conditions	4
2.3 Lattice Ward identities, Wick contractions, and flavour factors	5
3 Determination of $Z_S/(Z_P Z_A)$ from Ward identities	7
4 Numerical setup and results	10
4.1 Chiral extrapolation	11
4.2 Scaling	12
4.3 Interpolation formula	13
4.4 Comparison with previous works	13

5 Application: quark mass computations with Wilson fermions	15
5.1 Subtracted masses, PCAC masses, and redefined Symanzik counterterms	16
6 Conclusions	17
Appendix A: Basic definitions	18
Appendix B: Properties of $su(N_f)$ Lie algebra generators	18
Appendix C: Renormalisation and improvement	19
Appendix D: Charge conjugation, γ_5 -Hermiticity, and correlation functions	19
Appendix E: Non-perturbative checks	21
References	21

1 Introduction

Lattice QCD with Wilson fermions is a long-established regularisation. The fermionic action satisfies most desirable properties, namely strict locality, lack of fermion doublers, and preservation of flavour symmetry in a straightforward way. Well-known shortcomings are the presence of discretisation effects linear in the lattice spacing and, most importantly, the loss of chiral symmetry. The first problem is solved by applying the Symanzik-improvement programme (see for instance Ref. [1] for a review and Ref. [2] for more details). Chiral symmetry is recovered in the continuum, at the cost of having to deal with complicated renormalisation properties for most quantities of interest (cf. Ref. [3] and references therein; for a review see also Ref. [4]). A frequently cited example of these complications is the power divergence $m_{\text{crit}} \sim 1/a$, which must be subtracted from bare quark masses before they are renormalised multiplicatively. Other examples are the normalisation parameter Z_A of the axial current and the ratio Z_S/Z_P of the non-singlet scalar and pseudoscalar density renormalisation parameters. In a

^a e-mail: fabian.joswig@wwu.de (corresponding author)

regularisation scheme which respects chiral symmetry, these quantities are strictly equal to unity at finite values of the UV cutoff. With Wilson fermions these quantities are scale-independent finite functions of the gauge coupling, which tend to unity as we approach the continuum limit. In principle they are determined by requiring that chiral Ward identities at non-vanishing lattice spacing tend to their formal counterparts in the continuum limit. The scope of this paper is to provide a method for the determination of Z_S/Z_P based on Ward identities on physically small lattices with Schrödinger functional boundary conditions and realising a line of constant physics (LCP) in parameter space. Results are obtained for $N_f = 3$ dynamical quarks.

The general idea behind using chiral Ward identities in order to evaluate Z_S/Z_P for Wilson fermions appeared in Ref. [3].¹ It has been put to practice with quenched, unimproved Wilson fermions in Ref. [5] and subsequently with tree-level Symanzik-improved ones in Ref. [6]. The chiral Ward identities in question were obtained for large-volume lattices with periodic boundary conditions and non-chiral quark masses. Ratios of Z_S/Z_P were calculated at fixed gauge coupling for several quark masses and extrapolated to the chiral limit. A second-generation of calculations was not based on Ward identities but obtained by computing Z_S and Z_P in the RI/MOM scheme [7]. Again these calculations are performed at finite quark masses, followed by chiral extrapolations. A well known problem in this approach is that the Z_S/Z_P ratio thus obtained differs from the Ward identity one by “Goldstone pole contaminations” at the IR end of a renormalisation window. This problem was first identified in Ref. [7], and subsequently discussed in Refs. [8–11] (and reviewed in Ref. [4]), while the discussion specific to the difference between Ward identity and RI/MOM determinations of the ratio Z_S/Z_P is found in Ref. [10]. Although the problem is greatly attenuated by the RI/SMOM variant of this method [12], the requirement of a reliable renormalisation window is inherent in these approaches.

In the present work we revisit the Ward identity method, with an important novelty: lattices with small physical volumes and Schrödinger functional boundary conditions are used, with quark flavours degenerate in mass and (almost) at the chiral limit. In doing so, we follow closely the method introduced in Ref. [13] (and originally applied in the quenched approximation in that work) for the non-perturbative determination of the scale independent normalisation parameter Z_A of the axial vector current. Updates and optimisations of these computations can be found in refs. [14, 15] for two- and three-flavour QCD, respectively. Ward identities are imposed at constant physics to ensure a

removal of $O(a)$ effects in on-shell quantities and, at the same time, smoothly vanishing $O(a^2)$ effects as the bare coupling is varied. It must be stressed that the chiral Ward identities adopted in these works to determine Z_A are valid for $N_f \geq 2$ quark flavours, while the ones we introduce in the present work for the determination of $Z_S/(Z_P Z_A)$ are valid for $N_f \geq 3$.

We note in passing that, based on the chirally rotated Schrödinger functional construction of Ref. [16], a more recent method for the non-perturbative computation of Z_S/Z_P has been mentioned in Ref. [17].

This paper is organised as follows: in Sect. 2 (Sect. 2.1) we formally derive chiral Ward identities for continuum QCD, which relate correlation functions of non-singlet pseudoscalar and scalar composite operators (densities). The former are correlation functions with two operator insertions at two distinct space-time points (an axial current and a pseudoscalar density) in the presence of a generic external source operator. The latter involve a single insertion of the scalar operator. Subsequently (Sect. 2.2), we rewrite the same Ward identities in the lattice-regularised QCD with Wilson fermions. The external source consists of two standard Schrödinger functional boundary sources, each placed at a temporal boundary. The loss of chiral symmetry by Wilson fermions is taken into account by the renormalisation constants Z_P and Z_S of the pseudoscalar and scalar densities and the normalisation of the axial current, Z_A . In the chiral limit, these Ward identities hold up to $O(a^2)$ discretisation effects. We also discuss the corrections arising in practical simulations, which slightly deviate from the chiral limit; these are $O(am, a^2)$. Finally, in Sect. 2.3 we re-express these Ward identities in terms of traces of valence quark propagators, which multiply factored-out traces of generators of the $SU(N_f)$ flavour group.

Section 3 takes an even closer look at these Ward identities. We distinguish several equivalence classes, each consisting of identities with different flavour structure, which reduce to the same relations between correlation functions, giving the same $Z_S/(Z_P Z_A)$ result. Ward identities belonging to different equivalence classes provide $Z_S/(Z_P Z_A)$ estimates which differ by $O(am, a^2)$ effects. If we neglect these effects, we can combine identities from different equivalence classes, ending up with new relations between correlation functions (true up to $O(am, a^2)$ errors). Thus we can explore to what extent different equivalence classes provide independent estimates of $Z_S/(Z_P Z_A)$. Some of these estimates are expected to be noisier than others, as they are obtained using both quark-connected and quark-disconnected correlation functions.

In Sect. 4 we present our results for QCD with $N_f = 3$ dynamical flavours, where the lattice gauge action is tree-level Symanzik-improved and the fermion action is non-perturbatively Wilson–Clover improved. Our simulations are

¹ In practice, distinct chiral Ward identities are used for the computation of the ratio $Z_S/(Z_P Z_A)$ and Z_A ; the two results are subsequently multiplied to give Z_S/Z_P .

performed with degenerate mass flavours lying close to the chiral limit. The non-perturbative determination of the ratio Z_S/Z_P is carried out along a line of constant physics in parameter space. In practice, this requirement is met by ensuring a volume of almost constant spatial extent $L \sim 1.2$ fm in physical units, with Schrödinger functional boundary conditions. The ratio between temporal and spatial extent T/L is also kept fixed. This implies that any remaining intrinsic ambiguities in Z_S/Z_P of $O(a^2)$ or higher (in the $O(a)$ improved setup adopted here) disappear smoothly towards the continuum limit. The gauge couplings of our simulations span a range typical for the computations performed by the CLS (Coordinated Lattice Simulations) effort in QCD with $N_f = 2 + 1$ flavours of non-perturbatively improved Wilson fermions [18–21]. Our $Z_S/(Z_P Z_A)$ results are divided out by Z_A , estimated in Ref. [22]. Our Z_S/Z_P estimates are subsequently extrapolated to the chiral limit at fixed g_0^2 . Results are obtained from several Ward identities; they differ by discretisation effects. Thus it is possible to create ratios of the different Z_S/Z_P determinations, and plot them against (powers of) the lattice spacing, confirming the expected scaling behaviour. The statistically and systematically most precise Z_S/Z_P determination is parameterised as a continuous function of g_0^2 , which is our final answer. This is compared to two other determinations: one is based on ratios of PCAC quark masses with different flavours, employing essentially the same small-volume Schrödinger functional setup [23]; the other is based on the relation between bare current quark masses and bare subtracted quark masses, computed on large volumes with open boundary conditions [20].

Finally, in Sect. 5 we discuss how Z_S/Z_P can be used in quark mass determinations along the lines proposed in Ref. [24], but performing the mass renormalisation in the Schrödinger functional scheme and the renormalisation group running non-perturbatively, between renormalisation scales $\mu_{\text{had}} \sim \Lambda_{\text{QCD}}$ and $\mu_{\text{PT}} \sim M_W$. Such a calculation is subjected to different systematics than the standard ALPHA-CLS method, recently applied in Ref. [25].

Work in progress culminating to this paper had been reported in Refs. [26,27].

2 Chiral Ward identities for Z_S/Z_P

In this Section we will derive chiral Ward identities which relate correlation functions of non-singlet scalar and pseudoscalar composite operators (densities). These enable us to compute non-perturbatively the ratio Z_S/Z_P , which determines the relative normalisation of these scalar and pseudoscalar densities when the regularisation (Wilson fermion action) breaks chiral symmetry. First we will derive the pertinent chiral Ward identities in the formal continuum theory. Subsequently, we will show their lattice analogues with

Schrödinger functional boundary conditions. The resulting Ward identity computation of Z_S/Z_P follows very closely that of Z_A , described in refs. [13–15].

Our notation is pretty standard. Definitions of composite operators of dimension-3, axial transformations and Schrödinger functional (SF) boundary operators are collected in Appendix A. Conventions concerning the $su(N_f)$ flavour algebra are to be found in Appendix B. The lattice spacing is denoted by a , the (squared) gauge coupling by g_0^2 , and the inverse lattice coupling by $\beta \equiv 6/g_0^2$. Bare current (PCAC) and subtracted masses are defined in Appendix C.

2.1 Formal chiral Ward identities in the continuum

Under the small axial variations (A.8) of the fermion fields the formal, continuum QCD action in Euclidean space-time transforms as follows:

$$\begin{aligned} \delta_A S &= \int d^4x \left[(\partial_\mu \epsilon^a(x)) A_\mu^a(x) + i\epsilon^a(x) \bar{\psi}(x) \{T^a, M\} \gamma_5 \psi(x) \right] \\ &= \int d^4x \epsilon^a(x) \left[-\partial_\mu A_\mu^a(x) + 2m P^a(x) \right]. \end{aligned} \tag{1}$$

The fermion mass matrix is denoted by M . We work in the flavour symmetric (isospin) limit, so all quark masses m are degenerate. In the last expression we have integrated by parts the term with the axial current. Chiral Ward identities are obtained by considering that under the change of field variables defined in Eqs. (A.6), the expectation value of any composite operator \mathcal{O} (and products of them) is invariant. In the limit of small axial variations this leads to:

$$\begin{aligned} \delta_A \langle \mathcal{O} \rangle &= \frac{1}{Z} \delta_A \langle \int [\mathcal{D}\psi][\mathcal{D}\bar{\psi}][\mathcal{D}G_\mu] \mathcal{O} \exp(-S) \rangle = 0 \\ \Rightarrow \langle \delta_A \mathcal{O} \rangle &= \langle \mathcal{O} \delta_A S \rangle. \end{aligned} \tag{2}$$

We now take the axial variations to be non zero only in a space-time region R with a smooth boundary ∂R (i.e., for $x \in R$, $\epsilon^a(x) \neq 0$; otherwise $\epsilon^a(x) = 0$). The above expression reduces to

$$\int_R d^4x \epsilon^a(x) \left[\partial_\mu \langle A_\mu^a(x) \mathcal{O} \rangle - 2m \langle P^a(x) \mathcal{O} \rangle \right] = -\langle \delta_A \mathcal{O} \rangle. \tag{3}$$

We consider a product of composite operators $\mathcal{O} = P^b(y) \mathcal{O}_{\text{ext}}$, where $y \in R$ and \mathcal{O}_{ext} is defined outside the region R . This implies that $\delta_A \mathcal{O} = [\delta_A P^b(y)] \mathcal{O}_{\text{ext}}$. The pseudoscalar density $P^b(x)$ transforms as follows:

$$\delta_A P^b(x) = \epsilon^c(x) d^{cbe} S^e(x) + \epsilon^c(x) \frac{\delta^{cb}}{N_f} \bar{\psi}(x) \psi(x). \tag{4}$$

At this stage we impose that $\epsilon^c(x) = \epsilon \delta^{ac}$; i.e., it is a constant phase ϵ in a fixed direction a in flavour space, so that Ward identities become expressions reflecting *global* chiral symmetry. Moreover, in order to sidestep a number of complications,² we chose $a \neq b$, so that the last term on the r.h.s. of Eq. (4) drops out.³ Putting everything together, we obtain

$$\int_R d^4x \left[\partial_\mu \langle A_\mu^a(x) P^b(y) \mathcal{O}_{\text{ext}} \rangle - 2m \langle P^a(x) P^b(y) \mathcal{O}_{\text{ext}} \rangle \right] = -d^{abe} \langle S^e(y) \mathcal{O}_{\text{ext}} \rangle. \quad (5)$$

We note in passing that the first term is a surface term:

$$\int_R d^4x \partial_\mu \langle A_\mu^a(x) P^b(y) \mathcal{O}_{\text{ext}} \rangle = \int_{\partial R} d\sigma_\mu(x) \langle A_\mu^a(x) P^b(y) \mathcal{O}_{\text{ext}} \rangle. \quad (6)$$

As done in Ref. [13] for Z_A , we chose the region R to be the space-time volume between the hyper-planes at $y_0 - t$ and $y_0 + t$.⁴ Boundary conditions in space are periodic, implying $\int_R dx_0 d^3x \partial_k \langle A_k \dots \rangle = 0$. The Ward identity becomes

$$\int d^3\mathbf{x} \left[\langle A_0^a(y_0 + t; \mathbf{x}) - A_0^a(y_0 - t; \mathbf{x}) \rangle P^b(y_0; \mathbf{y}) \mathcal{O}_{\text{ext}} \right] - 2m \int d^3\mathbf{x} \int_{y_0-t}^{y_0+t} dx_0 \langle P^a(x_0; \mathbf{x}) P^b(y_0; \mathbf{y}) \mathcal{O}_{\text{ext}} \rangle = -d^{abe} \langle S^e(y) \mathcal{O}_{\text{ext}} \rangle. \quad (7)$$

It is convenient to introduce a spatial integration over \mathbf{y} :

$$\int d^3\mathbf{y} \int d^3\mathbf{x} \left[\langle A_0^a(y_0 + t; \mathbf{x}) - A_0^a(y_0 - t; \mathbf{x}) \rangle P^b(y_0; \mathbf{y}) \mathcal{O}_{\text{ext}} \right] - 2m \int d^3\mathbf{y} \int d^3\mathbf{x} \int_{y_0-t}^{y_0+t} dx_0 \langle P^a(x_0; \mathbf{x}) P^b(y_0; \mathbf{y}) \mathcal{O}_{\text{ext}} \rangle = -d^{abe} \int d^3\mathbf{y} \langle S^e(y) \mathcal{O}_{\text{ext}} \rangle. \quad (8)$$

The second line of the l.h.s. contains a contact term, arising when $r \equiv |x - y| \rightarrow 0$. The operator product is expressed in terms of an OPE (recall that $a \neq b$)

² With Wilson fermions, the singlet scalar operator $\bar{\psi}(x)\psi(x)$ mixes with the identity operator, introducing the complication of power divergences. Moreover, Wick contractions of the fermion fields of this operator generate quark-disconnected diagrams.

³ Here we are working with the algebra $su(N_f)$ for $N_f \geq 3$; for $N_f = 2$ we have that $d^{abe} = 0$ and the r.h.s. of Eq. (4) is trivial.

⁴ This choice of hyperplanes is made for simplicity. A more general choice, $y_0 - t_-$ and $y_0 + t_+$, with $t_- \neq t_+$ and $t_-, t_+ > 0$, is also acceptable.

$$P^a(x) P^b(y) \sim d^{abe} \sum_{k=1}^{\infty} C_k Q_k^e [D] r^{D-6} = d^{abe} C_1 S^e(x) r^{-3} + \dots, \quad (9)$$

where $[D]$ is the operator dimension and the Wilson coefficients C_k contain logarithms. The most divergent term in the OPE, taking into account the various symmetry properties of the operator product, is proportional to $S^e(x)$. The contribution to the space-time volume integral $2m \int_R \dots$ of a small four-sphere of centre x and radius a (or a small four-cube of size a) is then $\sim m \int_0^a dr r^3 r^{D-6} \langle \dots \rangle \sim m a^{D-2} \langle \dots \rangle$ and thus the leading term in the OPE contributes $O(am)$. In the lattice regularisation this implies that the contact term contributes an $O(am)$ discretisation effect to the Ward identity, even in a Symanzik-improved setup.

2.2 Lattice Ward identities with Schrödinger functional boundary conditions

We now adapt the previous formal manipulations to the lattice regularisation with Schrödinger functional boundary conditions. The external source for the Ward identity correlation functions is chosen to be a tensor in flavour space $\mathcal{O}_{\text{ext}}^{ad}$:

$$\mathcal{O}_{\text{ext}}^{ad} = \frac{1}{2L^6} \mathcal{O}^a \mathcal{O}^d, \quad (10)$$

with \mathcal{O}^a and \mathcal{O}^d defined in Eqs. (A.9). With this source and in lattice notation the Ward identity (8) becomes (with $b \neq c$):

$$Z_A Z_P a^6 \times \left\{ \sum_{\mathbf{x}, \mathbf{y}} \langle \mathcal{O}^a \left[(A_1)_0^b(y_0 + t; \mathbf{x}) - (A_1)_0^b(y_0 - t; \mathbf{x}) \right] P^c(y_0; \mathbf{y}) \mathcal{O}^d \right\rangle - 2ma \sum_{\mathbf{x}, \mathbf{y}} \sum_{x_0=y_0-t}^{y_0+t} w(x_0) \langle \mathcal{O}^a P^b(x_0; \mathbf{x}) P^c(y_0; \mathbf{y}) \mathcal{O}^d \rangle \right\} = -d^{bce} Z_S a^3 \sum_{\mathbf{y}} \langle \mathcal{O}^a S^e(y) \mathcal{O}^d \rangle + O(am, a^2). \quad (11)$$

In this expression, repeated flavour indices e are summed, as usual. The weight factor is $w(x_0) = 1/2$ for $x_0 = y_0 \pm t$ and $w(x_0) = 1$ otherwise. It is introduced in order to implement the trapezoidal rule for discretising integrals. The mass m is the current quark mass defined in Eq. (C.5); recall that we work with degenerate masses.

Assuming that we work in the chiral limit (or with nearly vanishing quark masses, so that $O(am)$ effects may be safely neglected), the above Ward identity is valid up to $O(a^2)$

cretisation errors in lattice QCD with Wilson quarks. Chiral symmetry breaking implies the (re)normalisation and improvement properties summarised in Appendix C. The Symanzik b -coefficients appearing in Eqs. (C.2)–(C.4) multiply the subtracted quark mass m_q or the quark mass matrix M_q . When working in or close to the chiral limit, as is the case in our simulations, we may safely drop these terms. Putting everything together we obtain Ward identity (11). The renormalisation factors of the external sources \mathcal{O}^a and \mathcal{O}^d are not taken into consideration, as they cancel out on both sides of the identity. Note that the term proportional to the current quark mass m may also be dropped in the chiral limit. In practice, since we are always working with masses that are not strictly zero, it turns out that it is advantageous to keep this term; see Ref. [15] and Sect. 4.1.

Equation (11) can be solved for $Z_S/(Z_P Z_A)$. With Z_A known either from other PCAC Ward identities [13–15] or from the chirally rotated Schrödinger functional formalism [22], we can thus obtain Z_S/Z_P .

2.3 Lattice Ward identities, Wick contractions, and flavour factors

Ward identity (11) relates expectation values of four composite operators on the l.h.s. to those of three composite operators on the r.h.s.; with a slight abuse of terminology, we call these four- and three-point correlation functions, respectively. We express these correlation functions, with Schrödinger functional boundary fields, in terms of traces of quark propagators. In standard ALPHA notation [28], $[\psi(y) \bar{\psi}(x)]_F$ denotes a quark propagator in a fixed background gauge field configuration, where x and y are space-time points in the bulk of the lattice. Propagators from the $x_0 = 0$ boundary to the bulk are $[\zeta(\mathbf{v}) \bar{\psi}(y)]_F$ (with \mathbf{v} a point at the $x_0 = 0$ boundary), while those from the $x_0 = T$ boundary to the bulk are $[\zeta'(\mathbf{v}') \bar{\psi}(y)]_F$ (with \mathbf{v}' a point at $x_0 = T$). Boundary-to-boundary propagators are $[\zeta'(\mathbf{v}') \bar{\zeta}(\mathbf{u})]_F$. For proper definitions see Ref. [28]. Note that, since we are working in the $su(N_f)$ -symmetric limit, all masses are degenerate and quark propagators of different flavours are indistinguishable.⁵

Performing the Wick contractions, we write the three-point correlation function of Eq. (11) as

$$a^3 \sum_y \langle \mathcal{O}^a S^e(y) \mathcal{O}^d \rangle = -ia^{15} \left(T^{dea} F_{S;1}(y_0) + T^{aed} F_{S;2}(y_0) \right), \tag{12}$$

⁵ The notation for fermion fields is somewhat ambiguous: for example, while in this Subsection $\psi(x)$, $\zeta(\mathbf{v})$, $\zeta'(\mathbf{v}')$ etc. stand for fields of a single flavour, in Appendix A the same quantities denote column vectors in flavour space. This ambiguity is fairly standard and should not create confusion.

where $T^{aed} \equiv \text{Tr}(T^a T^e T^d)$ are traces of three flavour $su(N_f)$ generators and $F_{S;1}(y_0)$, $F_{S;2}(y_0)$ are expectation values of traces of quark propagators with a scalar insertion. The exact expressions can be found in Table 1. Note that traces Tr act in flavour space, traces tr act in spin-colour space, and $\langle \dots \rangle$ denote averages over gauge field configurations. In Fig. 1 we show the quark-line diagrams corresponding to the spin-colour traces in the above equation. Any Wick contraction between fermion fields at the same point in the bulk $[\psi(y), \bar{\psi}(y)]_F$, or between boundary fields at the same time-slice (e.g. $[\zeta(\mathbf{v}) \bar{\zeta}(\mathbf{u})]_F$) gives rise to a quark-disconnected diagram,⁶ multiplied by the trace of an $su(N_f)$ generator. As this trace is zero, such diagrams do not contribute to the three-point correlation function. An example of such a diagram is shown in Fig. 1.

In Appendix D we combine the usual γ_5 -Hermiticity property of quark propagators, charge conjugation invariance of the lattice theory, and the trace properties of Eq. (B.4), to cast the r.h.s. of Eq. (12) into a single real term, and obtain for the r.h.s. of the Ward identity (11):

$$\text{WI r.h.s.} = -\frac{a^{15}}{2} Z_S d^{bce} d^{ade} \text{Re} \left[F_{S;1}(y_0) \right]. \tag{13}$$

Next we concentrate on the l.h.s. of Eq. (11). For simplicity we drop, for the moment, the term proportional to the quark mass. The l.h.s. consists of boundary-to-boundary correlation functions with two insertions of dimension-3 operators in the bulk, which can be cast in the general form

$$a^6 \sum_{\mathbf{x}, \mathbf{y}} \langle \mathcal{O}^a A_0^b(\mathbf{x}) P^c(\mathbf{y}) \mathcal{O}^d \rangle = a^{18} \sum_{k=1}^9 T_k^{abcd} F_{\text{AP};k}(x_0, y_0). \tag{14}$$

Upon performing the Wick contractions, each correlation function is expressed as the sum of 9 terms. They are products of traces of flavour matrices (denoted as T_k^{abcd}) and traces of loops of quark propagators averaged over gauge field configurations (denoted as $F_{\text{AP};k}(x_0, y_0)$). The former traces are defined as:

$$T_1^{abcd} \equiv \text{Tr}(T^a T^b T^c T^d), \quad T_2^{abcd} \equiv \text{Tr}(T^a T^d T^c T^b), \tag{15}$$

$$T_3^{abcd} \equiv \text{Tr}(T^a T^b T^d T^c), \quad T_4^{abcd} \equiv \text{Tr}(T^a T^c T^d T^b), \tag{16}$$

⁶ It is common practice to refer to these diagrams simply as disconnected. Since from a strict field-theoretic point of view they are connected (with multitudes of gluon lines, some of which contain fermion loops), the term quark-disconnected is more appropriate (valence-quark-disconnected would be even more accurate, but far too long). In the literature, quark-connected and quark-disconnected are sometimes referred to as one- and two-boundary diagrams.

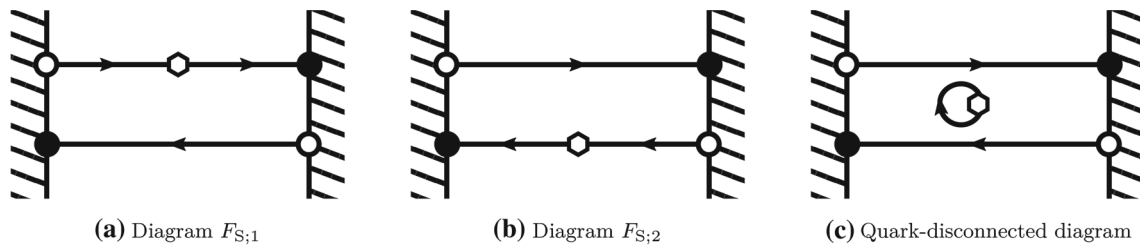


Fig. 1 The trace diagrams contributing to the expectation values of Table 1. The leftmost (rightmost) wall is time-slice $x_0 = 0$ ($x_0 = T$) with a γ_5 Dirac matrix between circles. The hexagons in the bulk represent the insertions of a scalar operator $S(y)$. The open circles correspond to the boundary fields ζ (at $x_0 = 0$) and ζ' (at $x_0 = T$), while the filled

circles denote $\bar{\zeta}$ (at $x_0 = 0$) and $\bar{\zeta}'$ (at $x_0 = T$). Quark-connected diagrams $F_{S;1}$ and $F_{S;2}$ are single traces, formed by starting from any point and following the lines (quark propagators) around until we close the loop. The quark-disconnected diagram is a product of two traces

Table 1 Mathematical expressions for the diagrams $F_{S;k}$ depicted in Fig. 1 and the diagrams $F_{AP;k}$ depicted in Fig. 2

$$\begin{aligned}
 F_{S;1}(y_0) &= \sum_y \sum_{\mathbf{u}, \mathbf{v}, \mathbf{u}', \mathbf{v}'} \langle \text{tr} \{ [\zeta'(\mathbf{v}') \bar{\zeta}(\mathbf{u})]_{F\gamma_5} [\zeta(\mathbf{v}) \bar{\psi}(y)]_F [\psi(y) \bar{\zeta}'(\mathbf{u}')]_{F\gamma_5} \} \rangle \\
 F_{S;2}(y_0) &= \sum_y \sum_{\mathbf{u}, \mathbf{v}, \mathbf{u}', \mathbf{v}'} \langle \text{tr} \{ [\zeta'(\mathbf{v}') \bar{\psi}(y)]_F [\psi(y) \bar{\zeta}(\mathbf{u})]_{F\gamma_5} [\zeta(\mathbf{v}) \bar{\zeta}'(\mathbf{u}')]_{F\gamma_5} \} \rangle \\
 F_{AP;1}(x_0, y_0) &= - \sum_{\mathbf{x}, \mathbf{y}} \sum_{\mathbf{u}, \mathbf{v}, \mathbf{u}', \mathbf{v}'} \langle \text{tr} \{ [\zeta'(\mathbf{v}') \bar{\psi}(x)]_{\gamma_0 \gamma_5} [\psi(x) \bar{\psi}(y)]_{\gamma_5} [\psi(y) \bar{\zeta}(\mathbf{u})]_{\gamma_5} [\zeta(\mathbf{v}) \bar{\zeta}'(\mathbf{u}')]_{\gamma_5} \} \rangle \\
 F_{AP;2}(x_0, y_0) &= - \sum_{\mathbf{x}, \mathbf{y}} \sum_{\mathbf{u}, \mathbf{v}, \mathbf{u}', \mathbf{v}'} \langle \text{tr} \{ [\zeta'(\mathbf{v}') \bar{\zeta}(\mathbf{u})]_{\gamma_5} [\zeta(\mathbf{v}) \bar{\psi}(y)]_{\gamma_5} [\psi(y) \bar{\psi}(x)]_{\gamma_0 \gamma_5} [\psi(x) \bar{\zeta}'(\mathbf{u}')]_{\gamma_5} \} \rangle \\
 F_{AP;3}(x_0, y_0) &= - \sum_{\mathbf{x}, \mathbf{y}} \sum_{\mathbf{u}, \mathbf{v}, \mathbf{u}', \mathbf{v}'} \langle \text{tr} \{ [\zeta'(\mathbf{v}') \bar{\psi}(x)]_{\gamma_0 \gamma_5} [\psi(x) \bar{\zeta}(\mathbf{u})]_{\gamma_5} [\zeta(\mathbf{v}) \bar{\psi}(y)]_{\gamma_5} [\psi(y) \bar{\zeta}'(\mathbf{u}')]_{\gamma_5} \} \rangle \\
 F_{AP;4}(x_0, y_0) &= - \sum_{\mathbf{x}, \mathbf{y}} \sum_{\mathbf{u}, \mathbf{v}, \mathbf{u}', \mathbf{v}'} \langle \text{tr} \{ [\zeta'(\mathbf{v}') \bar{\psi}(y)]_{\gamma_5} [\psi(y) \bar{\zeta}(\mathbf{u})]_{\gamma_5} [\zeta(\mathbf{v}) \bar{\psi}(x)]_{\gamma_0 \gamma_5} [\psi(x) \bar{\zeta}'(\mathbf{u}')]_{\gamma_5} \} \rangle \\
 F_{AP;5}(x_0, y_0) &= - \sum_{\mathbf{x}, \mathbf{y}} \sum_{\mathbf{u}, \mathbf{v}, \mathbf{u}', \mathbf{v}'} \langle \text{tr} \{ [\zeta'(\mathbf{v}') \bar{\psi}(y)]_{\gamma_5} [\psi(y) \bar{\psi}(x)]_{\gamma_0 \gamma_5} [\psi(x) \bar{\zeta}(\mathbf{u})]_{\gamma_5} [\zeta(\mathbf{v}) \bar{\zeta}'(\mathbf{u}')]_{\gamma_5} \} \rangle \\
 F_{AP;6}(x_0, y_0) &= - \sum_{\mathbf{x}, \mathbf{y}} \sum_{\mathbf{u}, \mathbf{v}, \mathbf{u}', \mathbf{v}'} \langle \text{tr} \{ [\zeta'(\mathbf{v}') \bar{\zeta}(\mathbf{u})]_{\gamma_5} [\zeta(\mathbf{v}) \bar{\psi}(x)]_{\gamma_0 \gamma_5} [\psi(x) \bar{\psi}(y)]_{\gamma_5} [\psi(y) \bar{\zeta}'(\mathbf{u}')]_{\gamma_5} \} \rangle \\
 F_{AP;7}(x_0, y_0) &= + \sum_{\mathbf{x}, \mathbf{y}} \sum_{\mathbf{u}, \mathbf{v}, \mathbf{u}', \mathbf{v}'} \langle \text{tr} \{ [\zeta'(\mathbf{v}') \bar{\psi}(x)]_{\gamma_0 \gamma_5} [\psi(x) \bar{\zeta}'(\mathbf{u}')]_{\gamma_5} \} \text{tr} \{ [\psi(y) \bar{\zeta}(\mathbf{u})]_{\gamma_5} [\zeta(\mathbf{v}) \bar{\psi}(y)]_{\gamma_5} \} \rangle \\
 F_{AP;8}(x_0, y_0) &= + \sum_{\mathbf{x}, \mathbf{y}} \sum_{\mathbf{u}, \mathbf{v}, \mathbf{u}', \mathbf{v}'} \langle \text{tr} \{ [\zeta'(\mathbf{v}') \bar{\psi}(y)]_{\gamma_5} [\psi(y) \bar{\zeta}'(\mathbf{u}')]_{\gamma_5} \} \text{tr} \{ [\psi(x) \bar{\zeta}(\mathbf{u})]_{\gamma_5} [\zeta(\mathbf{v}) \bar{\psi}(x)]_{\gamma_0 \gamma_5} \} \rangle \\
 F_{AP;9}(x_0, y_0) &= + \sum_{\mathbf{x}, \mathbf{y}} \sum_{\mathbf{u}, \mathbf{v}, \mathbf{u}', \mathbf{v}'} \langle \text{tr} \{ [\zeta'(\mathbf{v}') \bar{\zeta}(\mathbf{u})]_{\gamma_5} [\zeta(\mathbf{v}) \bar{\zeta}'(\mathbf{u}')]_{\gamma_5} \} \text{tr} \{ [\psi(x) \bar{\psi}(y)]_{\gamma_5} [\psi(y) \bar{\psi}(x)]_{\gamma_0 \gamma_5} \} \rangle
 \end{aligned}$$

$$T_5^{abcd} \equiv \text{Tr}(T^a T^c T^b T^d), \quad T_6^{abcd} \equiv \text{Tr}(T^a T^d T^b T^c), \tag{17}$$

$$T_7^{abcd} \equiv \text{Tr}(T^a T^b) \text{Tr}(T^d T^c), \tag{18}$$

$$T_8^{abcd} \equiv \text{Tr}(T^a T^c) \text{Tr}(T^d T^b), \tag{19}$$

$$T_9^{abcd} \equiv \text{Tr}(T^a T^d) \text{Tr}(T^c T^b), \tag{20}$$

$$+ \left. \sum_{k=7}^8 T_k^{abcd} \left\{ F_{AP;k}(y_0 + t, y_0) - F_{AP;k}(y_0 - t, y_0) \right\} \right]. \tag{21}$$

Note that correlation functions $F_{AP;k}$ are real for $k = 1, \dots, 9$. See Appendix D for more details. We will use a somewhat more compact notation, defining

$$\Delta_k(y_0, t) \equiv F_{AP;k}(y_0 + t, y_0) - F_{AP;k}(y_0 - t, y_0). \tag{22}$$

while the latter ones are also given in Table 1.

The spin-colour trace diagrams are shown in Fig. 2. We see that there are six quark-connected diagrams, and three quark-disconnected ones. The condition $b \neq c$ implies that $T_9 F_{AP;9}(x_0, y_0) = 0$, due to the vanishing of $\text{Tr}(T^c T^b)$. From Eq. (B.2) we see that T_k^{abcd} for $k = 7, 8$ are real.

Once more we combine γ_5 -Hermiticity, charge conjugation invariance, and Eq. (B.5), to obtain for the l.h.s. of the Ward identity (11):

Collecting Eqs. (13), (21), and (22), we write the Ward identity (11) in the chiral limit as:

$$\begin{aligned}
 a^3 Z_A Z_P & \\
 & \times \left[\sum_{k=1,3,5} 2\text{Re}(T_k^{abcd}) \Delta_k(y_0, t) + \sum_{k=7,8} T_k^{abcd} \Delta_k(y_0, t) \right] \\
 & = - \frac{Z_S}{2} d^{bce} d^{ade} \text{Re} \left[F_{S;1}(y_0) \right] + O(a^2). \tag{23}
 \end{aligned}$$

$$\begin{aligned}
 \text{WI l.h.s.} &= Z_A Z_P a^{18} \\
 & \times \left[\sum_{k=1,3,5} 2\text{Re}(T_k^{abcd}) \left\{ F_{AP;k}(y_0 + t, y_0) - F_{AP;k}(y_0 - t, y_0) \right\} \right]
 \end{aligned}$$

In order to keep the equation simple, we have not shown the mass-dependent terms with two pseudoscalar density insertions, appearing in Eq. (11). These terms are included in the numerical analysis, which is carried out close to, but

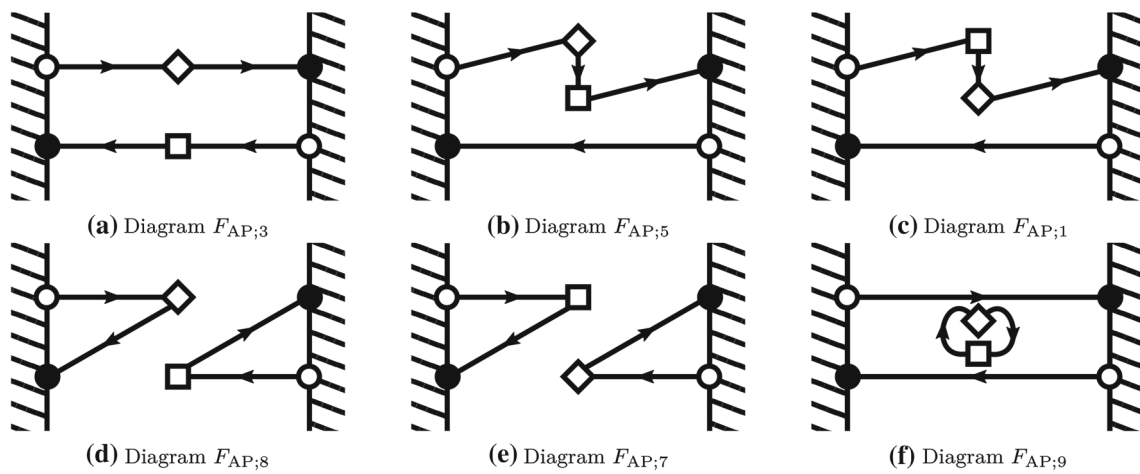


Fig. 2 The trace diagrams contributing to the expectation values of Table 1. Conventions are similar to those of Fig. 1. The diamonds in the bulk represent the insertions of a pseudoscalar operator $P(y)$. The squares in the bulk represent the insertions of an axial current $A_0(x)$ or a pseudoscalar operator $P(x)$ (giving rise to the Dirac matrices $\gamma_0\gamma_5$ or γ_5 , respectively). Quark-connected diagrams $F_{AP;3}$, $F_{AP;5}$, $F_{AP;1}$

are single traces, formed by starting from any point and following the lines (quark propagators) around until we close the loop. Quark-disconnected diagrams $F_{AP;8}$, $F_{AP;7}$, $F_{AP;9}$ are products of two traces. Diagrams $F_{AP;2}$, $F_{AP;4}$, $F_{AP;6}$ are not shown, as they are related to $F_{AP;1}$, $F_{AP;3}$, $F_{AP;5}$; cf. Eqs. (D.5)

not strictly at the chiral limit. The reader should have no difficulty convincing himself that they are exactly analogous to $F_{AP;k}(y_0 + t, y_0)$ and $F_{AP;k}(y_0 - t, y_0)$ appearing above. Their net effect is to add extra mass-dependent contributions to the $\Delta_k(y_0, t)$ functions. From now on, the $\Delta_k(y_0, t)$ functions are meant to include these contributions, proportional to the quark mass. Consequently, the uncertainty on the r.h.s. of Eq. (23) becomes $O(am, a^2)$.

It is interesting to compare the Ward identities we have derived here to the one introduced in Ref. [13] for the determination of Z_A . The former are valid for $N_f \geq 3$, while the latter for $N_f \geq 2$. The Ward identity of Ref. [13] involves correlation functions with two axial current insertions in the bulk. In our case we have more complicated contributions, consisting of time-differences of correlation functions with one axial current and one pseudoscalar density insertion.

3 Determination of $Z_S/(Z_P Z_A)$ from Ward identities

Ward identity (23) is a master equation, from which a plethora of relations arise for specific choices of flavour indices a, b, c, d . In what follows, each of them will be distinguished by the label $WI(abcd)$. Not all of them are suitable for the determination of Z_S/Z_P . The following constraints need to be imposed:

- (i) $b \neq c$; this ensures the suppression of the scalar term in Eq. (4);
- (ii) $d^{bce} \neq 0$ and $d^{ade} \neq 0$, so that the r.h.s. of Eq. (23) does not vanish. Note that once b, c are fixed, property A in Appendix B ensures that $d^{bce} \neq 0$ for a single value of

e . Thus the summation over e on the r.h.s. of our master equation is trivial and the requirement $d^{bce}d^{ade} \neq 0$ is satisfied for at most a single value of e ;

- (iii) $f^{bce} = 0$ for the choice of indices b, c, e for which $d^{bce} \neq 0$; $f^{ade} = 0$ for the choice of indices a, d, e for which $d^{ade} \neq 0$. This follows from property B in Appendix B.

In spite of these constraints, a lot of freedom remains in the choice of flavour indices, resulting in many Ward identities. They are relations between the correlation functions of the master equation, which can be solved for $Z_S/(Z_P Z_A)$. These Ward identities can be grouped into different equivalence classes. Each class consists of several identities $WI(abcd)$ with different flavour indices a, \dots, d , but identical flavour factors $\text{Re}(T_k)$ ($k = 1, 3, 5, 7, 8$), and thus the same Eq. (23). Therefore, the same $Z_S/(Z_P Z_A)$ estimate is obtained from all Ward identities of the same equivalence class. Estimates of $Z_S/(Z_P Z_A)$ from Ward identities of different classes differ by discretisation effects.

The combinations of conditions (i)–(iii) simmer down to the choice of flavour indices (a, b, c, d) , with $b \neq c$, such that $d^{bce}d^{ade} \neq 0$. We systematically investigated the choices of flavour indices which fulfill these conditions with a computer algebra program and grouped them into the equivalence classes which are tabulated in Table 2. These results depend on the $su(N_f)$ Gell–Mann matrix definitions of Appendix B. Some interesting observations are:

- There are pairs of equivalence classes that have the same number of elements. Examples are $WI(1245)$ paired to $WI(1425)$, $WI(1144)$ paired to $WI(1414)$ etc. These pairs

Table 2 Ward identities $WI(abcd)$ grouped into equivalence classes. Each class is labeled by four flavour indices $abcd$, of a representative element, listed in the leftmost column. All elements of the same class are grouped to the right. For more explanations, see text

Equivalence class label	Equivalence class elements
1245	1245 1254 1267 1276 1346 1357 1364 1375 2145 2154 2167 2176 2347 2356 2365 2374 3146 3157 3164 3175 3247 3256 3265 3274 4512 4521 4567 4576 4613 4631 4723 4732 5412 5421 5467 5476 5623 5632 5713 5731 6413 6431 6523 6532 6712 6721 6745 6754 7423 7432 7513 7531 7612 7621 7645 7654
1425	1425 1436 1524 1537 1627 1634 1726 1735 2415 2437 2514 2536 2617 2635 2716 2734 3416 3427 3517 3526 3614 3625 3715 3724 4152 4163 4251 4273 4361 4372 4657 4756 5142 5173 5241 5263 5362 5371 5647 5746 6143 6172 6253 6271 6341 6352 6475 6574 7153 7162 7243 7261 7342 7351 7465 7564
1486	1486 1587 1684 1785 2487 2586 2685 2784 3484 3585 3686 3787 4168 4278 4348 4843 4861 4872 5178 5268 5358 5853 5862 5871 6148 6258 6368 6841 6852 6863 7158 7248 7378 7842 7851 7873 8416 8427 8434 8517 8526 8535 8614 8625 8636 8715 8724 8737
1846	1846 1857 1864 1875 2847 2856 2865 2874 3844 3855 3866 3877 4438 4483 4618 4681 4728 4782 5538 5583 5628 5682 5718 5781 6418 6481 6528 6582 6638 6683 7428 7482 7518 7581 7738 7783 8146 8157 8164 8175 8247 8256 8265 8274 8344 8355 8366 8377
1468	1468 1578 1648 1758 2478 2568 2658 2748 4186 4287 4384 4816 4827 4834 5187 5286 5385 5817 5826 5835 6184 6285 6386 6814 6825 6836 7185 7284 7387 7815 7824 7837 8461 8472 8562 8571 8641 8652 8742 8751
1144	1144 1155 1166 1177 2244 2255 2266 2277 3344 3355 3366 3377 4411 4422 4433 4466 4477 5511 5522 5533 5566 5577 6611 6622 6633 6644 6655 7711 7722 7733 7744 7755
1414	1414 1515 1616 1717 2424 2525 2626 2727 3434 3535 3636 3737 4141 4242 4343 4646 4747 5151 5252 5353 5656 5757 6161 6262 6363 6464 6565 7171 7272 7373 7474 7575
1188	1188 2288 3388 8811 8822 8833
1818	1818 2828 3838 8181 8282 8383
4488	4488 5588 6688 7788 8844 8855 8866 8877
4848	4848 5858 6868 7878 8484 8585 8686 8787

Table 3 Classes of Ward identities (first column), the corresponding flavour factors of Eq. (23) (columns 2 to 6) and the product of symmetric tensors d of the same equation (last column)

WI(abcd)	$Re(T_1^{abcd})$	$Re(T_3^{abcd})$	$Re(T_5^{abcd})$	T_7^{abcd}	T_8^{abcd}	$d^{bce}d^{ade}$
WI(1245)	-1/16	1/16	0	0	0	-1/4
WI(1425)	0	1/16	-1/16	0	0	-1/4
WI(1486)	$-\sqrt{3}/24$	$\sqrt{3}/48$	$\sqrt{3}/48$	0	0	$-\sqrt{3}/12$
WI(1846)	$\sqrt{3}/48$	$\sqrt{3}/48$	$-\sqrt{3}/24$	0	0	$-\sqrt{3}/12$
WI(1468)	$\sqrt{3}/48$	$-\sqrt{3}/24$	$\sqrt{3}/48$	0	0	$\sqrt{3}/6$
WI(1144)	1/16	1/16	0	1/4	0	1/4
WI(1414)	0	1/16	1/16	0	1/4	1/4
WI(1188)	1/24	1/24	1/24	1/4	0	1/3
WI(1818)	1/24	1/24	1/24	0	1/4	1/3
WI(4488)	5/48	5/48	-1/12	1/4	0	1/12
WI(4848)	-1/12	5/48	5/48	0	1/4	1/12

of classes are separated by a single horizontal line in Table 2. Class WI(1468) does not have a partner.

- The flavour factors $Re(T_k)$ for $(k = 1, 3, 5)$, T_7 , and T_8 of paired classes have closely related numerical values; see Table 3. We will see below how this leads to useful relations between certain Δ_k functions.
- The quark disconnected traces Δ_7 and Δ_8 do not contribute to the equivalence classes of the top half of Table 2 (separated by a triple line from the bottom half).

In Table 3 we collect the flavour factors $Re(T_k)$ ($k = 1, 3, 5)$, T_7 , and T_8 for each class. Depending on the choice of flavour indices a, b, c, d , some of these flavour factors vanish. This simplifies the resulting Ward identity. Also here the top part of the Table (separated by a double line from the bot-

tom half) lists the Ward identities without Δ_7 - and Δ_8 -type contributions.

There are two possible ways of using the 11 Ward identities of Table 3. A first approach would be to determine $Z_S/(Z_P Z_A)$ from each of the 11 variants of Eq. (23). In principle these determinations differ by $O(am, a^2)$ effects and that should provide a handle for a good control of the related systematics. However, in practice the different $Z_S/(Z_P Z_A)$ results are all obtained from the same configuration ensembles and are thus strongly correlated. Moreover, paired Ward identities (in the sense discussed above; cf. Table 2) have very similar relations between their Δ_k -terms and this also leads to very similar Z -ratios.

A second approach would be to combine these Ward identities in order to first obtain relations between the various Δ_k -terms. These would be true up to $O(am, a^2)$ at fixed gauge coupling, and once established, would simplify the equation(s) relating $Z_S/(Z_P Z_A)$ to the Δ_k 's. In this spirit we proceed as follows:

- (i) Starting from Ward identities without quark disconnected contributions (i.e., with $\text{Re}(T_7) = \text{Re}(T_8) = 0$; top part of Table 3), we combine the pair WI(1245) and WI(1425) to obtain:

$$\Delta_1(y_0, t) = \Delta_5(y_0, t) + O(am, a^2), \tag{24}$$

$$Z_A Z_P a^3 [\Delta_1(y_0, t) - \Delta_3(y_0, t)] = -2 Z_S \text{Re} [F_{S;1}(y_0)] + O(am, a^2). \tag{25}$$

Note that by combining the pair WI(1486) and WI(1846) we also obtain the above expressions, so this pair does not provide extra information.

- (ii) WI(1468), which has no partner, is written, in terms of the Δ 's defined in Eq. (22), as:

$$Z_A Z_P a^3 [\Delta_1(y_0, t) - 2\Delta_3(y_0, t) + \Delta_5(y_0, t)] = -2 Z_S \text{Re} [F_{S;1}(y_0)] + O(am, a^2). \tag{26}$$

This on its own determines the ratio $Z_S/(Z_P Z_A)$. Note that combined with Eq. (24), it gives us Eq. (25). Our conclusion is that all Ward identities with $\text{Re}(T_7) = \text{Re}(T_8) = 0$ reduce to the equality $\Delta_1 = \Delta_5$ (i.e., diagrams $F_{AP;1}$ and $F_{AP;5}$ of Fig. 2 are related) and a single Ward identity, from which $Z_S/(Z_P Z_A)$ may be computed.

- (iii) Passing to Ward identities with quark-disconnected contributions (bottom part of Table 3), we combine the pair WI(1188) and WI(1818) to obtain:

$$\Delta_7(y_0, t) = \Delta_8(y_0, t) + O(am, a^2), \tag{27}$$

$$Z_A Z_P a^3 [2\Delta_1(y_0, t) + \Delta_3(y_0, t) + 3\Delta_7(y_0, t)]$$

$$= -2 Z_S \text{Re} [F_{S;1}(y_0)] + O(am, a^2), \tag{28}$$

where Eq. (24) has also been used to arrive at Eq. (28).

- (iv) Similarly, the pair WI(1144) and WI(1414) combine to give

$$\Delta_1(y_0, t) + 2\Delta_7(y_0, t) = \Delta_5(y_0, t) + 2\Delta_8(y_0, t) + O(am, a^2), \tag{29}$$

$$Z_A Z_P a^3 [2\Delta_1(y_0, t) + \Delta_3(y_0, t) + 2\Delta_7(y_0, t)] = -2 Z_S \text{Re} [F_{S;1}(y_0)] + O(am, a^2). \tag{30}$$

Eq. (29) carries no new information, as it is a combination of Eqs. (24) and (27).

- (v) If we now combine Eqs. (28) and (30), we obtain again Eq. (25) and the new relation

$$\Delta_3(y_0, t) = -\Delta_7(y_0, t) + O(am, a^2). \tag{31}$$

The bottom line is that, up to $O(am, a^2)$ discretisation effects, the 11 Ward identities corresponding to the entries of Table 3 are not all independent. They can be combined to give three relations between the functions Δ_k , which depend on traces of valence quark propagators, without references to flavour traces; these are Eqs. (24), (27), and (31).⁷ The extent to which these relations are fulfilled at non-zero lattice spacing is an indicator of the size of discretisation effects. Moreover, if we take them at face value, the remaining Ward identities (25), (26), (28), and (30) reduce to a single expression. Any of them can be used to provide estimates of the ratio $Z_S/(Z_P Z_A)$. We expect Eqs. (28), and (30) to be noisier, as they involve quark-disconnected diagrams. Eq. (25) seems promising, as it only involves Δ_1 and Δ_3 , but it cannot be excluded *a priori* that Eq. (28) turns out to be better behaved. This can only be decided by numerical investigation.

Of course, these considerations do not exhaust all possibilities. Any linear combination of the Ward identities considered above, possibly combined with the relations (24), (27), (31), can be used for the computation of $Z_S/(Z_P Z_A)$. For example, the linear combination $L_1 \equiv [\text{WI}(1245) - \text{WI}(1425)]$, combined with Eq. (24) gives:

$$Z_A Z_P a^3 [\Delta_1(y_0, t)] = -Z_S \text{Re} [F_{S;1}(y_0)] + O(am, a^2). \tag{32}$$

The determination of $Z_S/(Z_P Z_A)$ from the above depends only on quark-connected diagrams. Similarly, the linear com-

⁷ As an aside we note that Eqs. (24) and (27) relate correlation functions of similar topology (quark-connected or quark-disconnected ones). On the contrary, Eq. (31) is more intriguing, as it relates quark-connected to quark-disconnected diagrams.

bination $L_2 \equiv [12\text{WI}(1818) - 8\text{WI}(1414)]$ gives:

$$\begin{aligned} Z_A Z_P a^3 [\Delta_1(y_0, t) + \Delta_8(y_0, t)] \\ = -Z_S \text{Re} [F_{S;1}(y_0)] + O(am, a^2), \end{aligned} \quad (33)$$

which yields a $Z_S/(Z_P Z_A)$ estimate from quark-connected and quark-disconnected diagrams. The last two expressions will be used in the following for numerical crosschecks.

4 Numerical setup and results

We investigate the proposed Ward identities on lattices with tree-level Symanzik improved gluons and Wilson-Clover quarks. The action coincides with the one used by CLS [18,20,21]. We employ Schrödinger functional boundary conditions in time, which enable us to simulate at quark masses close to the chiral point and control systematic effects related to the massless renormalisation framework. The details of this aspect are discussed in Sect. 4.1. Similar to the procedure in [15], we construct boundary-to-boundary three- and four-point functions with pseudoscalar Schrödinger functional wall sources and use wavefunctions at the boundaries as explained in [29]. The statistical error analysis is performed using a python implementation of the Γ -method [30] (exploiting information from the autocorrelation function) with automatic differentiation [31].

The gauge ensembles used in this study are detailed in Table 4. They coincide with the ones used in [23] but for the ensemble C1k1. These are essentially the ensembles used in [15,29] plus the ensembles A1k3, A1k4, B1k4, C1k1, D1k2 and D1k4, which were added to improve the chiral fits. For the two ensembles E1k1 and E1k2 the number of molecular dynamics units was increased by factor of more than 4. The ensembles with volume $L^3 \times T$ described above are designed to lie on a line of constant physics (LCP), where the spatial extent of $L \approx 1.2$ fm and $T/L \approx 3/2$ are almost constant. The Ward identity conditions which fix the ratio $Z_S/(Z_P Z_A)$ are imposed at constant physics, i.e., we require that all length scales in the correlation functions, which define a given condition formulated through one of the foregoing Ward identities, are kept fixed in physical units. Once this requirement is satisfied, only the lattice spacing a changes as g_0 is varied. Consequently, renormalisation constants (as well as their ratios) extracted from different constant physics conditions are expected to rapidly approach an almost unique function of g_0 as $g_0 \rightarrow 0$. For a more general discussion of the constant physics idea in a similar context see, e.g., Ref. [32].

The initial tuning of this LCP was done based on the (universal) 2-loop beta-function as explained in Ref. [29]. Thus the volume of the lattices varies by $\approx 10\%$ over the range of couplings considered. However, using the results of Ref. [19],

we verified that this deviation is proportional to the lattice spacing a and thus contributes to our quantity of interest only as a higher-order ambiguity.⁸

The simulations in this work suffer from critical slowing down of the topological charge for smaller lattice spacings. This phenomenon, often dubbed “topology freezing”, could give unreliable results due to an insufficient sampling of topological sectors. We circumvent this problem by reweighting all data to the trivial topological sector $Q = 0$ at the cost of decreasing the effective number of configurations; see [29,34] for a discussion. Furthermore we increase the statistical uncertainties by attaching a tail to the integrated autocorrelation functions as proposed in [35]. As measure for τ_{exp} , the autocorrelation time of the slowest mode in the simulation, we use the integrated autocorrelation time of the squared topological charge Q^2 extracted from the longest Monte Carlo chain for each value of β . The τ_{exp} -values for the individual ensembles can be found in Table 4.

In order to solve the Ward identity for Z_S/Z_P we need non-perturbative knowledge of the non-singlet axial current renormalisation constant Z_A and the $O(a)$ improvement coefficient c_A . The constant Z_A was calculated on a subset of the gauge configurations in this work, Ref. [15], as well as in the chirally rotated Schrödinger functional, Ref. [22], which is a completely different determination. We prefer the results from the latter because of their smaller statistical uncertainties. The errors of Z_A are accounted for in quadrature when solving for Z_S/Z_P in our Ward identity expressions. For c_A we use the results of [29], without error, following standard practice.

In principle the ratio we would like to determine, as well as all correlation functions involved, depend on the $O(a)$ improved coupling $\tilde{g}_0^2 = g_0^2[1 + ab_g \text{tr} M_q/N_f]$, where the coefficient b_g is only known at 1-loop perturbation theory [2]. This issue is of no relevance here, as all normalisation conditions are imposed at zero quark mass. However, this should be kept in mind when using results obtained here in a different setting with non-vanishing sea quark masses.

In order to study the scaling behaviour of some of our results, we need the lattice spacings in physical units at the bare couplings used in this work. In Ref. [19], such values are provided for couplings close to those in Table 4; these enable us to extract the lattice spacings at our gauge couplings using a polynomial interpolation.

As additional cross checks we investigate the non-perturbative validity of the identities (24), (27) and (31). The results can be found in Appendix E.

⁸ A more explicit quantitative investigation of violations of the constant physical volume requirement by our Schrödinger functional ensembles, demonstrating that it affects the Ward identity determination of improvement coefficients and normalisation factors only beyond the order we are actually interested in, will be reported in [33].

Table 4 Summary of simulation parameters: the first column (ID) labels our gauge configuration ensembles, the second column lists the lattice sizes $L^3 \times T/a^4$, the third one the inverse gauge couplings β , the fourth the Wilson hopping parameters κ , the fifth shows the total number of molecular dynamics units MDU, the sixth the autocorrelation time of the slowest mode τ_{exp} , and the last one the corresponding lattice spacing a , estimated from Ref. [19]

ID	$L^3 \times T/a^4$	β	κ	MDU	τ_{exp}	a in fm
A1k1	$12^3 \times 17$	3.3	0.13652	20480	1.031(71)	0.1045(18)
A1k3	$12^3 \times 17$	3.3	0.13648	6876	2.06(14)	0.1045(18)
A1k4	$12^3 \times 17$	3.3	0.1365	96640	1.031(71)	0.1045(18)
E1k1	$14^3 \times 21$	3.414	0.1369	38400	1.61(12)	0.08381(68)
E1k2	$14^3 \times 21$	3.414	0.13695	57600	1.61(12)	0.08381(68)
B1k1	$16^3 \times 23$	3.512	0.137	20480	4.41(96)	0.06954(43)
B1k2	$16^3 \times 23$	3.512	0.13703	8192	4.41(96)	0.06954(43)
B1k3	$16^3 \times 23$	3.512	0.1371	16384	4.41(96)	0.06954(43)
B1k4	$16^3 \times 23$	3.512	0.13714	27856	4.41(96)	0.06954(43)
C1k1	$20^3 \times 29$	3.676	0.1368	7848	10.7(4.1)	0.05170(42)
C1k2	$20^3 \times 29$	3.676	0.137	15232	10.7(4.1)	0.05170(42)
C1k3	$20^3 \times 29$	3.676	0.13719	15472	10.7(4.1)	0.05170(42)
D1k2	$24^3 \times 35$	3.81	0.13701	5360	62(14)	0.04175(70)
D1k4	$24^3 \times 35$	3.81	0.137033	79664	31.0(7.0)	0.04175(70)

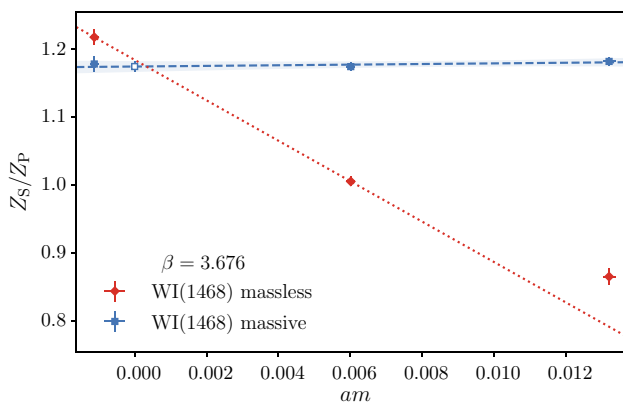


Fig. 3 Comparison of the chiral extrapolation for WI(1468) at $\beta = 3.676$ with and without the term proportional to the mass. In the massless case the data cannot be described by a linear function in am for the full mass range. The dotted line visualises the chiral extrapolation of the massless data set excluding the outmost data point. When the mass term is included, the data shows no significant quark mass dependence. The slope of the linear fit function, shown as the dashed line, where the shaded area corresponds to the 1σ uncertainty, is zero within error

4.1 Chiral extrapolation

From the plethora of possible renormalisation conditions listed in Sect. 3, we single out a class labeled WI(1468) to which only quark connected diagrams contribute and for which the statistical precision is best. We detail the analysis for this specific choice, but the same steps also apply to any other identity discussed in the following.

In order to obtain Z_S/Z_P at vanishing quark mass, we extra- or interpolate the data at fixed bare coupling to the chiral point. For this procedure we employ the $O(a)$ improved PCAC mass, which we average over the central third of the temporal extent of the lattice, similarly to what was done in

Ref. [23]. This choice keeps the plateau length approximately constant in physical units. For the insertion times in the master Eq. (23), we chose $y_0 = T/2$ and $t = T/6$ rounded up to the closest integer.⁹ The idea behind this choice is to place the operators as far away from the temporal boundaries as possible, so as to suppress boundary induced cutoff effects, while keeping the individual operators apart from each other, thus avoiding contact terms.

In Fig. 3 we show the chiral extrapolation of our preferred determination WI(1468), at $\beta = 3.676$, where quark masses cover a large range in lattice units. We compare results obtained from the Ward identity with and without the mass term [i.e., the term with two pseudoscalar insertions in Eq. (11)]. We see that in the “massive” case our results display a linear behaviour in the whole mass range. In addition statistical uncertainties are smaller and the data show an almost flat dependence on am , resulting to a more reliable chiral extrapolation. Therefore, we obtain Z_S/Z_P in the chiral limit by fitting linearly the results of the “massive” case. For this fit we employ orthogonal distance regression [36] which takes into account not only errors in the dependent, but also in the independent variable. The error obtained from this procedure for the chirally extrapolated Z_S/Z_P is in general larger compared to the one obtained from a standard least squares fit. Results for the individual ensembles as well as the chiral extrapolations are summarised in Table 5, which will be discussed in Sect. 4.2.

⁹ As discussed in Ref. [15], the temporal extent of our lattices is odd, so there is no central time-slice.

Table 5 Summary of results for am and Z_S/Z_P from different Ward identity determinations, labelled by $WI(abcd)$. The Ward identity linear combinations L_1 and L_2 are defined in Eqs. (32) and (33). In all Ward identities the mass terms with two pseudoscalar insertions in the bulk have been included; cf. eq. (11). The errors quoted for the individual ensembles are statistical; the uncertainty on the values at the chiral point stem from the orthogonal distance regression procedure of Ref. [36]

ID	am	WI(1468)	WI(1245)	L_1	WI(4488)	L_2
A1k1	-0.00282(62)	1.550(28)	1.554(46)	1.662(53)	2.320(493)	1.688(76)
A1k3	0.00127(91)	1.513(50)	1.469(48)	1.863(86)	1.439(814)	1.570(130)
A1k4	-0.00113(34)	1.510(39)	1.519(62)	2.120(147)	2.712(348)	1.685(47)
	0.0	1.514(32)	1.495(34)	1.863(83)	2.244(453)	1.644(63)
E1k1	0.00269(20)	1.359(14)	1.337(16)	1.527(33)	1.679(216)	1.450(39)
E1k2	-0.00017(17)	1.333(14)	1.323(17)	1.497(38)	1.937(184)	1.452(32)
	0.0	1.334(13)	1.324(16)	1.498(36)	1.922(175)	1.452(30)
B1k1	0.00554(20)	1.257(10)	1.259(14)	1.346(17)	1.456(148)	1.267(26)
B1k2	0.00444(31)	1.249(17)	1.236(22)	1.352(29)	1.088(242)	1.234(36)
B1k3	0.00110(21)	1.272(13)	1.272(14)	1.337(20)	1.374(150)	1.314(32)
B1k4	-0.00056(16)	1.250(9)	1.248(11)	1.312(24)	1.667(162)	1.327(27)
	0.0	1.255(8)	1.255(9)	1.323(17)	1.528(117)	1.320(21)
C1k1	0.01320(17)	1.182(6)	1.176(7)	1.191(8)	0.793(124)	1.150(32)
C1k2	0.00601(12)	1.174(7)	1.172(10)	1.200(12)	1.250(140)	1.171(21)
C1k3	-0.00112(12)	1.178(11)	1.178(12)	1.198(17)	1.190(129)	1.166(15)
	0.0	1.174(8)	1.176(10)	1.200(13)	1.236(109)	1.167(13)
D1k2	0.00074(22)	1.145(25)	1.149(24)	1.157(20)	1.202(322)	1.147(41)
D1k4	-0.00007(4)	1.143(2)	1.143(6)	1.148(6)	1.147(31)	1.144(5)
	0.0	1.143(3)	1.144(5)	1.148(6)	1.152(39)	1.144(6)

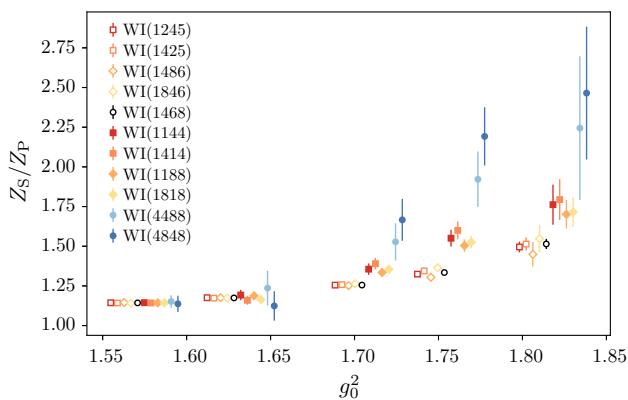


Fig. 4 Dependence of Z_S/Z_P on the gauge coupling g_0^2 . Results are obtained from the 11 Ward identity classes listed in Table 3. Open symbols are used for the Ward identity classes with connected-quark diagrams only; closed symbols denote Ward identity classes with both connected- and disconnected-quark diagrams. Closely related Ward identities (which are separated by a single horizontal line in Table 2) are shown with the same symbol. Data from WI(1144) are shown at their exact abscissa position, while the others have been slightly displaced in the g_0^2 -direction, in order to improve visibility

4.2 Scaling

In Table 3 we have listed 11 classes of distinct Ward identities; each of them is a different relation between correlation function differences Δ_k ($k = 1, 3, 5, 7, 8$) and $F_{S;1}$, from which Z_S/Z_P may be obtained. In Fig. 4 we show these determinations in the chiral limit as functions of the gauge

coupling g_0^2 . It is evident, as argued in Sect. 3, that there are very strong correlations between results obtained on the same configuration ensembles from “similar” Ward identity classes, as grouped in Table 2.

We are thus led to select, from the plethora of Ward identities, four representative determinations of Z_S/Z_P . Two of these involve only quark connected diagrams. These are WI(1245) and the linear combination L_1 , leading to Eq. (32). The other two determinations involve both quark connected and disconnected diagrams and are therefore numerically more challenging. Here we chose WI(4488), and the linear combination L_2 , leading to Eq. (33). The results for each ensemble and in the chiral limit are shown in Table 5.

To evaluate the relative cutoff effects among our different results, we form ratios of Z_S/Z_P , obtained from each of the four determinations described above, to Z_S/Z_P from our preferred identity WI(1468). We investigate the lattice spacing dependence of each of these four ratios which, in our Symanzik-improved setup, consists of powers of a^2 and higher. The ratios are known to tend to unity in the continuum limit. We therefore fit them with polynomials in the lattice spacing, constrained to be 1 at the origin. Results are displayed in Fig. 5. The top panel of the figure displays results from the first two determinations, without quark disconnected contributions.

The deviations from 1 in the ratio WI(1245)/WI(1468) are very mild and can be described by a single term quadratic in the lattice spacing with $\chi^2/\text{d.o.f} = 0.474$. For the ratio $L_1/\text{WI}(1468)$ the deviation from 1 as well as the statistical

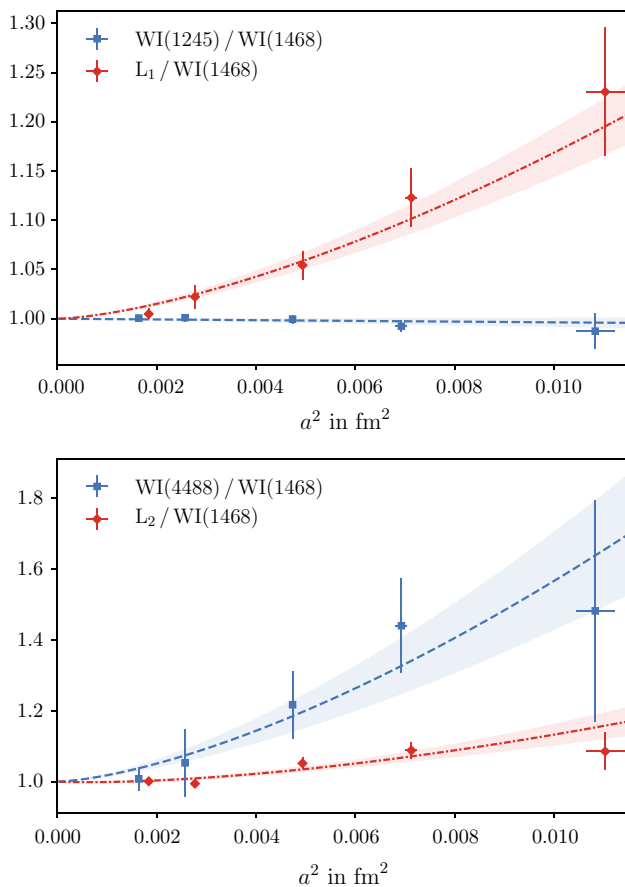


Fig. 5 Lattice spacing dependence of the ratio of different Z_S/Z_P determinations to Z_S/Z_P from WI(1468). The top panel depicts results from Ward identities which involve quark-connected diagrams only, while the bottom panel shows results from Ward identities which also involve quark-disconnected diagrams

uncertainties are larger. A glance at Fig. 5 should convince the reader that the data cannot be described by a single-parameter fit with a quadratic term. Fitting with $1 + c_2 a^2 + c_3 a^3$ results to $c_2 = -9.3(4.3)$, $c_3 = 303(71)$ and $\chi^2/\text{d.o.f} = 0.138$. A one-parameter fit with a term proportional to a^3 gives $c_3 = 169(22)$ with $\chi^2/\text{d.o.f} = 0.775$; this is the curve shown in Fig. 5. The bottom panel of Fig. 5 displays results from the determinations with quark disconnected contributions. Again it is obvious that none of the data displays a pure a^2 -dependence. Fitting the ratio WI(4488)/WI(1468) with $1 + c_2 a^2 + c_3 a^3$ results to $c_2 = -26(28)$, $c_3 = 911(410)$ and $\chi^2/\text{d.o.f} = 0.494$; note that c_2 is compatible with zero. Fitting by $1 + c_3 a^3$ gives $c_3 = 567(131)$ and $\chi^2/\text{d.o.f} = 0.511$; this is the fit shown in the Figure. For the ratio $L_2/\text{WI}(1468)$ we again fit with two parameters, one quadratic and one cubic in the lattice spacing, obtaining $c_2 = -7.8(4.6)$, $c_3 = 211(68)$ and $\chi^2/\text{d.o.f} = 1.719$. The relatively large value for $\chi^2/\text{d.o.f}$ can be traced to the data point at the coarsest lattice spacing. All four cases conform with the theoretical expectation of $O(a^2)$ ambiguities or higher. We did not find

any evidence for $O(a)$ cutoff effects; trying to fit an additional term proportional to a gives coefficients which are zero within errors.

4.3 Interpolation formula

To facilitate the use of our Z_S/Z_P results in large volume simulations, we provide an interpolation formula for lattice spacings $0.04 \text{ fm} \lesssim a \lesssim 0.1 \text{ fm}$. Having tried several fit ansätze, we opt for a Padé interpolation constrained by the 1-loop value [37] of the form

$$\left(\frac{Z_S}{Z_P}\right)(g_0^2) = 1 + 0.020164 g_0^2 \times \frac{1 - Z_{\text{SP}}^{(0)} g_0^2 + Z_{\text{SP}}^{(1)} g_0^4}{1 - Z_{\text{SP}}^{(2)} g_0^2}, \quad (34a)$$

$$Z_{\text{SP}}^{(0)} = -0.5357, \quad Z_{\text{SP}}^{(1)} = 0.2883, \quad Z_{\text{SP}}^{(2)} = -0.5117, \quad (34b)$$

with the covariance matrix

$$\text{cov}(Z_{\text{SP}}^{(i)}, Z_{\text{SP}}^{(j)}) = \begin{pmatrix} +2.0195e-01 & -1.3844e-01 & -4.1248e-03 \\ -1.3844e-01 & +9.5121e-02 & +2.8754e-03 \\ -4.1248e-03 & +2.8754e-03 & +9.6128e-05 \end{pmatrix}, \quad (34c)$$

and $\chi^2/\text{d.o.f} = 0.169$.

As the functional form in the non-perturbative coupling region is in principle unknown, we investigated the significance of systematic effects by also experimenting with alternative forms of interpolating functions (such as higher-order Padés, exponentials and polynomials), constrained to monotonically approach the 1-loop perturbation theory result. However, among those describing our results reliably (as signaled by an acceptable $\chi^2/\text{d.o.f}$) practically coincide with the interpolation (34) in the fitted range of couplings, so that the associated systematic errors are negligible compared to the statistical ones. Therefore, we only account for systematic uncertainties when extrapolating with Eq. (34) to values slightly outside the fitted range by adding a systematic error of 50% of the size of the statistical one in quadrature. This prescription is applied at $\beta = 3.85$, which corresponds to the finest lattice spacing simulated by the CLS effort.

The WI(1468) results with the interpolation are shown in Fig. 6, where they are also compared to the prediction of 1-loop perturbation theory. The vertical dashed lines mark the bare couplings used in CLS simulations, to which we want to interpolate our results. Results for Z_S/Z_P at the g_0^2 -values used in $N_f = 2 + 1$ CLS simulations are given in Table 6.

4.4 Comparison with previous works

We are not aware of any direct determinations of Z_S/Z_P in our specific setup, but we can compare our findings,

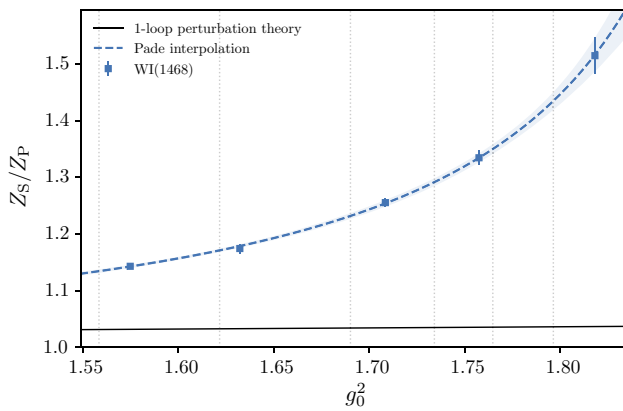


Fig. 6 Z_S/Z_P results from WI(1468), extrapolated to the chiral point, plotted against the bare gauge coupling g_0^2 . The Padé interpolation formula (34), shown with errorband, is used to propagate the statistical uncertainty. The 1-loop perturbative result from Ref. [37] is shown for comparison. The vertical dashed lines indicate the CLS couplings of Refs. [18,20,21]

Table 6 Z_S/Z_P results from WI(1468) (second column) and from Ref. [23] for two lines of constant physics (LCP), specified there. The inverse gauge couplings β are those used in $N_f = 2 + 1$ CLS simulations [18,20,21]. The error of the WI(1468) results is the statistical uncertainty propagated from the interpolation formula (34) except for $\beta = 3.85$ where we added a systematic uncertainty, 50% of the size of the statistical one, in quadrature. For the results of the two LCP columns we combine the errors of Z (from Ref. [23]) and Z_A (from Ref. [22]) in quadrature

β	WI(1468)	[23] LCP-0	[23] LCP-1
3.85	1.1343(25)	1.1437(33)	1.1441(24)
3.7	1.1709(23)	1.2047(34)	1.2023(25)
3.55	1.2317(48)	1.3073(72)	1.2971(51)
3.46	1.2914(64)	1.409(10)	1.3866(70)
3.4	1.3497(83)	1.509(12)	1.4720(77)
3.34	1.435(15)	1.662(19)	1.595(11)

using existing results for the quark mass renormalisation constant $Z \equiv Z_P/(Z_S Z_A)$. The idea is to compute $Z_S/Z_P = (Z Z_A)^{-1}$, with Z from either Ref. [20] or Ref. [23], and Z_A from Ref. [22]. In Ref. [20], Z has been computed on large-volume CLS ensembles, from the relation between PCAC quark masses m_{ij} and subtracted quark masses $m_{q,ij}$ (see Sect. 5 and Appendix C for these mass definitions). The Z -results in Ref. [23] were obtained on almost the same gauge ensembles used in this work¹⁰ at small volumes and nearly-chiral sea quark masses. The method of Ref. [23] is based on suitable combinations of renormalised quark masses, defined both through the PCAC relation and the subtracted bare mass, evaluated in the $O(a)$ improved theory with non-degenerate valence quarks, including all necessary counterterms. Results

¹⁰ We additionally use ensemble C1k1.

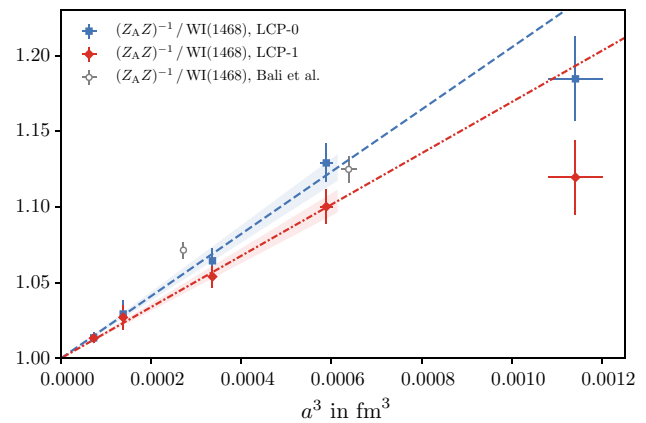


Fig. 7 Scaling behaviour of the ratio of Z_S/Z_P deduced from results in Refs. [20,23] to Z_S/Z_P from WI(1468)

are quoted for two different lines of constant physics labeled LCP-0 and LCP-1, which differ by the values at which the quark masses in the valence sector are kept fixed as g_0 is varied.

We compute the ratio of $1/(Z Z_A)$ from Refs. [20] and [23] to Z_S/Z_P from our preferred WI(1468). We investigate the lattice spacing dependence of this ratio, which consists of powers of a^2 and higher, and tends to unity in the continuum limit. The results are plotted in Fig. 7. Polynomial fits are performed on the LCP-0 and LCP-1 ratios, excluding the data of the coarsest ensembles, which display poor scaling behaviour and large errors. A two-parameter fit of the form $1 + c_2 a^2 + c_3 a^3$ results to $\chi^2/\text{d.o.f} = 0.281$, $c_2 = -2.5(3.7)$ and $c_3 = 242(57)$ for LCP-0, and $\chi^2/\text{d.o.f} = 0.166$, $c_2 = 1.5(2.8)$ and $c_3 = 148(45)$ for LCP-1, in both cases c_2 is consistent with zero. We thus prefer to plot the results as functions of a^3 in Fig. 7, where we also show a one-parameter fit of the form $1 + c_3 a^3$; for this ansatz we obtain $\chi^2/\text{d.o.f} = 0.300$, $c_3 = 206(14)$ for LCP-0 and $\chi^2/\text{d.o.f} = 0.170$, $c_3 = 169(12)$ for LCP-1.¹¹ We interpret this as confirmation that the two methods are compatible w.r.t. the expected lattice spacing ambiguities and that the effects of $O(a^2)$ are subdominant compared to the next higher order.

Let us briefly comment on the possible benefits of the respective results on Z_S/Z_P collected in Table 6, originating from the different approaches underlying Ref. [23] and this work. First, one observes comparable uncertainties between the two. While the method of that reference involves combinations of simpler and thus typically less noisy correlation functions (i.e., with only one operator insertion in the bulk) as well as an accurate computation of the valence quark mass dependence prior to the chiral extrapolations, our estimates on Z_S/Z_P from the more direct Ward identity approach fol-

¹¹ Since we neglect correlations between our results and those of Ref. [23], the error in their ratio is probably overestimated. This explains the small values of $\chi^2/\text{d.o.f}$.

lowed here exhibit an overall flatter and, at larger couplings, less steep g_0^2 -dependence. This points to generically smaller cutoff effects so that continuum extrapolations of quantities where it enters may be expected to become better controlled and more precise in the long run, because they are also less affected by unpleasantly significant admixtures of higher-order cutoff effects.

The results for Z presented in [20], stemming from large-volume calculations on a subset of the CLS ensembles, are only available at two values of the bare coupling, which do not coincide with the couplings investigated in this work. In order to compare with our results we make use of the interpolation formula Eq. (34). Although the estimates for Z from Ref. [20] are only available at two values of the bare coupling and we hence do not attempt a fit in this case, we notice that they are compatible with LCP-0.

In summary, comparison with earlier works is consistent with the expectation that all ambiguities between different determinations of Z_S/Z_P show a scaling according to $O(a^2)$ or higher. However, the size of these ambiguities is quite large and may still have a relevant impact on applications as described in the next Section.

5 Application: quark mass computations with Wilson fermions

We will now discuss a method of computing quark masses with Wilson fermions which uses the ratio Z_S/Z_P .

First we review the well-established ‘‘PCAC quark mass method’’. It is the conventional ALPHA Collaboration approach, which relies on the PCAC definition of quark masses m_{ij} of Eq. (C.7). These bare current masses are computed on large physical volumes¹² and for a range of couplings typical of hadronic, low-energy scales $\mu_{\text{had}} \sim \Lambda_{\text{QCD}}$. Although we keep our notation as general as possible, for concreteness we consider a theory with $N_f = 2 + 1$ dynamical fermions; i.e. the two lightest flavours are degenerate in mass while the third flavour is heavier ($m_{q,1} = m_{q,2} < m_{q,3}$).

We see from Eq. (C.8) that the renormalised light mass is given by

$$m_{1,R} = m_{2,R} = \frac{Z_A}{Z_P} m_{12} \times \left[1 + (b_A - b_P)am_{q,12} + (\bar{b}_A - \bar{b}_P)a \text{Tr}(M_q) \right] + O(a^2). \tag{35}$$

¹² The ALPHA Collaboration has performed these calculations for quenched QCD with Schrödinger functional boundary conditions; see Ref. [38]. The CLS effort determined quark masses for $N_f = 2$ QCD with periodic boundary conditions [39,40] and for $N_f = 2 + 1$ QCD with open boundary conditions [25,41].

The ratio of the heavy to light renormalised masses is also derived from the above expression:

$$\frac{m_{3,R}}{m_{1,R}} = 2 \frac{m_{13}}{m_{12}} \left[1 + (b_A - b_P) \frac{(am_{q,3} - am_{q,2})}{2} \right] - 1 + O(a^2). \tag{36}$$

Knowing the renormalised light mass from Eq. (35), and the ratio of the heavy and light renormalised masses from Eq. (36), the up/down and strange masses are obtained [19, 25]. So *in principle* this method requires:

1. The axial current normalisation $Z_A(g_0^2)$ and the renormalisation constant $Z_P(g_0^2, \mu_{\text{had}})$ of the non-singlet pseudoscalar density; the latter carries the renormalisation scheme and scale dependence of the continuum quark mass. In our $N_f = 3$ setup, these may be found in Refs. [22] and [42], respectively.
2. The Symanzik-improvement coefficients $(b_A - b_P)$ and $(\bar{b}_A - \bar{b}_P)$. Non-perturbative $(b_A - b_P)$ -estimates in our setup may be found in Ref. [23]. Note that in perturbation theory $(\bar{b}_A - \bar{b}_P) \sim O(g_0^4)$, so that the term proportional to this coefficient is habitually dropped.
3. It is also noteworthy that Eq. (36) does not require knowledge of κ_{crit} , which is however needed in $m_{q,12}$ and $\text{Tr}(M_q)$ in Eq. (35). We shall return to this point in Sect. 5.1.

Based on the results of Ref. [43] for Symanzik-improved quark masses with Wilson fermions, an alternative approach, known as the ‘‘ratio-difference method’’, has been proposed in Ref. [24]. The renormalised quark mass difference is given by

$$m_{3,R} - m_{1,R} = Z_S^{-1} \left[m_{q,3} - m_{q,1} \right] \times \left[1 + a2b_m m_{q,13} + a\bar{b}_m \text{Tr}(M_q) \right] + O(a^2). \tag{37}$$

Knowing the renormalised mass difference from Eq. (37), and the ratio of the heavy and light renormalised masses from Eq. (36), the up/down and strange masses are obtained. So *in principle* this method requires:

1. The renormalisation constant $Z_S(g_0^2, \mu_{\text{had}})$ of the non-singlet scalar density, which carries the renormalisation scheme and scale dependence of the continuum quark mass.
2. The Symanzik-improvement coefficients $(b_A - b_P)$, b_m and \bar{b}_m . Non-perturbative estimates of the b_m -coefficient in this setup may be found in Ref. [23].¹³ Since $\bar{b}_m \sim$

¹³ In perturbation theory $2b_m = -1 + O(g_0^2)$ and the non-perturbative estimates of Ref. [23] are also numerically sizeable. Thus this Symanzik

$O(g_0^4)$, the term proportional to $\text{Tr}(M_q)$ is habitually dropped.

3. The critical hopping parameter κ_{crit} is needed in $m_{q,13}$ and $\text{Tr}(M_q)$ in Eq. (37). We shall return to this point in Sect. 5.1.

We have outlined the basic idea behind the PCAC quark mass method and the ratio-difference method, listing the renormalisation parameters and improvement coefficients required by each one. The most crucial difference is that in the PCAC quark mass method all bare masses are given in terms of the current masses m_{12} and m_{13} , which are renormalised by $Z_P^{-1}Z_A$, while in the ratio-difference method the bare mass difference is the exactly known $[m_{q,3} - m_{q,1}]$, which is renormalised by Z_S^{-1} . It is not possible to determine Z_S with a Schrödinger functional renormalisation condition analogous to that introduced in Ref. [44] for Z_P . The latter involves correlation functions with a pseudoscalar source at the boundary (see Eq. (A.9)) and the pseudoscalar scalar operator at the bulk. If we place a scalar operator at the bulk, keeping the pseudoscalar boundary source, the correlation function vanishes due to parity. Nor is it possible to have a scalar source at the boundary and the scalar density at the bulk, since this would result in the product P_+P_- of the projection operators of the boundary quarks and the vanishing of the correlation function. An option would be to impose a renormalisation condition on the correlation function $\langle \mathcal{O}^a S^b(x) \mathcal{O}^c \rangle$, with the two pseudoscalar boundary sources \mathcal{O}^a and \mathcal{O}^c and the scalar operator S^b in the bulk. This would be an acceptable intermediate scheme of the Schrödinger functional variety, but different than the one introduced in Ref. [44] for Z_P . Thus, the renormalised quark masses m_{1R}, m_{3R} obtained by combining Eqs. (35) and (36) (PCAC quark mass method with Z_P) would be in a different scheme than those obtained from Eqs. (37) and (36) (difference-ratio method with Z_S). Only results obtained for the scheme-independent renormalisation group invariant (RGI) masses from the two methods would be comparable. This comparison would be very useful but cumbersome, as it requires the computation from scratch of the step scaling function in the new intermediate scheme, from ratios of Z_S 's at fixed renormalised coupling and two different renormalisation scales, and for a range of couplings.

Given the above considerations, we are led to define the scalar operator renormalisation parameter through:

$$Z_S(g_0^2, \mu_{\text{had}}) = \left[\frac{Z_S(g_0^2, \mu_{\text{had}})}{Z_P(g_0^2, \mu_{\text{had}})} \right] Z_P(g_0^2, \mu_{\text{had}}). \tag{38}$$

This is our definition of the Schrödinger functional renormalisation scheme for the scalar non-singlet operator. The

counterterm is expected to remove large $O(a)$ effects, especially in future computations of heavy flavour quark masses (charm etc.).

Z_S/Z_P -ratio on the r.h.s. is scale independent, being determined from Ward identities. Clearly, scalar and pseudoscalar densities have the same renormalisation group running properties (i.e., the same anomalous dimensions, the same step scaling functions in the continuum, etc.). So knowledge of the Z_S/Z_P ratio enables us to obtain the light and heavy quark masses in the usual Schrödinger functional scheme [44], but with a different method based on mass differences (and Z_S) combined with scale-independent PCAC mass ratios. The novel renormalisation and improvement patterns provide an important handle for the control and reduction of systematic effects related to the non-perturbative determination of renormalisation parameters and discretisation errors.¹⁴ What is common in both methods is the renormalisation group running that takes us non-perturbatively from renormalised masses at low energy scales μ_{had} to masses at large, perturbative scales $\mu_{\text{PT}} \sim M_W$, as described in Ref. [44]. For recent results on the running of quark masses in $N_f = 3$ QCD see Ref. [42].

5.1 Subtracted masses, PCAC masses, and redefined Symanzik counterterms

We will close this section by reviewing how, in both methods, we can circumvent the need to use κ_{crit} in the Symanzik counterterms of Eqs. (35) and (37), which feature subtracted masses $am_{q,ij}$ and $\text{Tr}[aM_q]$. This can be avoided by substituting these subtracted masses with current quark masses. Their relation is given by [43],

$$m_{ij} = Z \left[m_{q,ij} + (r_m - 1) \frac{\text{Tr}[M_q]}{N_f} \right] + O(a), \tag{39}$$

where $Z(g_0^2) \equiv Z_P/(Z_S Z_A)$ and $r_m \equiv Z_S/Z_{S_0}$ are finite normalisations (Z_{S_0} is the renormalisation parameter of the singlet scalar density). In the above we neglect $O(a)$ terms, as they only contribute to $O(a^2)$ in the b -counterterms of Eqs. (35) and (37). Substituting $am_{q,ij} \rightarrow am_{ij}$ in these expressions, we obtain respectively

$$m_{1,R} = m_{2,R} = \frac{Z_A}{Z_P} m_{12} \times \left[1 + (\bar{b}_A - \bar{b}_P)am_{12} + \left\{ (\bar{b}_A - \bar{b}_P) \frac{1 - r_m}{r_m} + (\bar{b}_A - \bar{b}_P) \frac{N_f}{Z r_m} \right\} \frac{aM_{\text{sum}}}{N_f} \right] + O(a^2), \tag{40}$$

and

$$m_{3,R} - m_{1,R} = Z_S^{-1} [m_{q,3} - m_{q,1}]$$

¹⁴ This could be crucial in computations of heavier quark masses (charm etc.), where the discretisation errors become dominant.

$$\begin{aligned} &\times \left[1 + 2\tilde{b}_m am_{13} \right. \\ &\left. + \left\{ 2\tilde{b}_m \frac{1-r_m}{r_m} + \tilde{b}_m \frac{N_f}{Zr_m} \right\} \frac{aM_{\text{sum}}}{N_f} \right] + O(a^2), \end{aligned} \quad (41)$$

where we define

$$\tilde{b}_A - \tilde{b}_P \equiv \frac{b_A - b_P}{Z}, \quad \tilde{b}_m \equiv \frac{b_m}{Z}, \quad (42)$$

$$\begin{aligned} M_{\text{sum}} &\equiv m_{12} + m_{23} + \dots + m_{(N_f-1)N_f} + m_{N_f} \\ &= Zr_m \text{Tr}[M_q] + O(a). \end{aligned} \quad (43)$$

Thus, $am_{q,ij}$ and κ_{crit} in Eqs. (35) and (37) have been traded off for m_{ij} , Z , and r_m . Accurate non-perturbative estimates of Z , $(b_A - b_P)$, and b_m in our $N_f = 3$ setup have been reported in Ref. [23]. The term multiplying M_{sum} contains $(1 - r_m)/r_m$ and $(\tilde{b}_A - \tilde{b}_P)$. To leading order in perturbation theory $r_m = 1 + 0.001158 C_F N_f g_0^4$ [20,45]; thus $(1 - r_m)/r_m \sim O(g_0^4)$. A first non-perturbative study of the coefficients \tilde{b}_A , \tilde{b}_P , and \tilde{b}_m produced noisy results with 100% errors [46]. Since in perturbation theory $(\tilde{b}_A - \tilde{b}_P)$, $\tilde{b}_m \sim O(g_0^4)$ [43], the terms proportional to M_{sum} are habitually dropped.

For completeness we also discuss a slightly different way to write the b_m -counterterm of the renormalised quark mass difference of Eq. (37), in close analogy to what is done in Ref. [24]. The term in question is written as follows:

$$\begin{aligned} ab_m[m_{q,3} + m_{q,1}] &= ab_m[m_{q,3} + m_{q,1}] \left[\frac{m_{q,3} - m_{q,1}}{m_{q,3} - m_{q,1}} \right] \\ &= ab_m \left[m_{q,3} - m_{q,1} \right] \frac{\left[\frac{m_{33'}}{m_{12}} + 1 \right] + \frac{2(1-r_m) M_{\text{sum}}}{r_m m_{12}}}{\left[\frac{m_{33'}}{m_{12}} - 1 \right]}. \end{aligned} \quad (44)$$

We arrive at the second expression using Eq. (39) and introducing the PCAC mass $m_{33'}$, which consists of two degenerate but distinct heavy valence flavours. Neglecting the term proportional to M_{sum} in Eq. (44), we conclude that in this approximation the difference-ratio method is based on Eqs. (36) and (37), which depend on the exactly known subtracted quark mass difference $[m_{q,3} - m_{q,1}]$ and suitable PCAC quark mass ratios, but not on subtracted quark mass averages $m_{q,ij}$ and κ_{crit} .

6 Conclusions

In the present study we have addressed, for the first time within the finite-volume Schrödinger functional setup, the non-perturbative determination of the ratio of the scalar to

pseudoscalar non-singlet renormalisation constants Z_S/Z_P in Wilson’s lattice QCD, exploiting suitable massive chiral Ward identities. We have shown that in lattice QCD with three flavours of Wilson-Clover quarks (with non-perturbative c_{sw} [47]) and tree-level Symanzik-improved gauge action, the Ward identities are restored up to $O(a^2)$ at finite lattice spacing. In order to ensure a smooth dependence of the renormalisation constant ratio on the bare gauge coupling, we have enforced a constant physics condition by working with an approximately fixed physical volume of spatial extent $L \approx 1.2$ fm and $T/L \approx 3/2$.

Our main results are the parameterisation of Z_S/Z_P in Eq. (34), valid for bare couplings $1.55 \lesssim g_0^2 \lesssim 1.85$ (i.e., lattice spacings 0.042 fm $\lesssim a \lesssim 0.105$ fm), as well as the values for Z_S/Z_P , given in Table 6, at the bare couplings typically employed in the large-volume $N_f = 2 + 1$ CLS ensembles [18–21]. On the technical level, we had to treat properly the topology freezing encountered in our simulations, principally at the finest lattice spacing, which may prevent a trustworthy estimation of the statistical error. The operator character of Ward identities ensures their validity in sectors of fixed topological charge. Thus we have projected the correlation functions entering the Ward identities onto the trivial topological sector throughout our analysis.

Several checks have been performed, in order to guarantee the stability of the analysis and a careful assessment of the statistical as well as the systematic errors. In particular, we have verified that results on Z_S/Z_P from the different classes of Ward identities at our disposal are perfectly consistent with each other as expected, i.e., up to ambiguities of $O(a^2)$ or even higher. Among the various estimators for $[Z_S/Z_P](g_0^2)$, our preferred choice, advocated in Eq. (34), was guided by the structural simplicity of the underlying chiral Ward identity, its numerical precision, and its robustness against systematic effects.

Since the range of couplings covered in this work matches those of the large-volume gauge field configurations generated by CLS with the same lattice action, our result for $[Z_S/Z_P](g_0^2)$, combined with the scale dependent renormalisation factor Z_P from [42], can be used in the computation of quark masses as outlined in Sect. 5. Work in this direction, extending the $(2 + 1)$ -flavour computations of light, strange and charm quark masses on the CLS ensembles reported in refs. [25,41], is in progress.

Acknowledgements We thank Stefan Sint, Christian Wittemeier, Carl Christian Köster and Simon Kuberski for helpful discussions and especially Carl for his valuable contributions in extending the set of ensembles used in our computations. A. V. wishes to thank the Particle Physics Theory Group at WWU Münster and Trinity College Dublin for their hospitality. This work is supported by the Deutsche Forschungsgemeinschaft (DFG) through the Research Training Group GRK 2149: *Strong and Weak Interactions – from Hadrons to Dark Matter* (F. J. and J. H.). We acknowledge the computer resources provided by the Zentrum

für Informationsverarbeitung of the University of Münster (PALMA & PALMA II HPC clusters) and thank its staff for support.

Data Availability Statement This manuscript has no associated data or the data will not be deposited. [Authors' comment: The data on which the conclusions of this article rely are reported in the tables to ensure the reproduction of our results. Further underlying datasets generated during and/or analysed during the current study and supporting the data in the tables are available from the corresponding author on reasonable request.]

Open Access This article is licensed under a Creative Commons Attribution 4.0 International License, which permits use, sharing, adaptation, distribution and reproduction in any medium or format, as long as you give appropriate credit to the original author(s) and the source, provide a link to the Creative Commons licence, and indicate if changes were made. The images or other third party material in this article are included in the article's Creative Commons licence, unless indicated otherwise in a credit line to the material. If material is not included in the article's Creative Commons licence and your intended use is not permitted by statutory regulation or exceeds the permitted use, you will need to obtain permission directly from the copyright holder. To view a copy of this licence, visit <http://creativecommons.org/licenses/by/4.0/>. Funded by SCOAP³.

Appendix A: Basic definitions

We define non-singlet vector and axial vector currents in QCD with N_f quarks as

$$V_\mu^a(x) = i\bar{\psi}(x)\gamma_\mu T^a \psi(x), \quad (\text{A.1})$$

$$A_\mu^a(x) = i\bar{\psi}(x)\gamma_\mu \gamma_5 T^a \psi(x), \quad (\text{A.2})$$

with $a = 1, \dots, (N_f^2 - 1)$ an $SU(N_f)$ flavour index. See Appendix B for our conventions regarding $SU(N_f)$ groups and $su(N_f)$ Lie algebras. Analogously, non-singlet scalar and pseudoscalar densities are given by

$$S^a(x) = i\bar{\psi}(x)T^a \psi(x), \quad (\text{A.3})$$

$$P^a(x) = i\bar{\psi}(x)\gamma_5 T^a \psi(x). \quad (\text{A.4})$$

Axial transformations of the fermion fields are defined as:

$$\psi(x) \rightarrow \psi'(x) = \exp\left[i\epsilon^a(x)T^a \gamma_5\right] \psi(x), \quad (\text{A.5})$$

$$\bar{\psi}(x) \rightarrow \bar{\psi}'(x) = \bar{\psi}(x) \exp\left[i\epsilon^a(x)T^a \gamma_5\right]. \quad (\text{A.6})$$

Small axial field variations are obtained by expanding the above up to $O(\epsilon)$:

$$\delta_A \psi(x) = \epsilon^a(x) \delta_A^a \psi(x) \approx i\epsilon^a(x) T^a \gamma_5 \psi(x), \quad (\text{A.7})$$

$$\delta_A \bar{\psi}(x) = \epsilon^a(x) \delta_A^a \bar{\psi}(x) \approx i\epsilon^a(x) \bar{\psi}(x) T^a \gamma_5. \quad (\text{A.8})$$

Note that in general these transformations are defined to be *local* (i.e., ϵ^a depends on space-time). Their *global* counterparts are related to symmetries of the continuum theory (vector and chiral).

In the Schrödinger functional framework, standard zero-momentum sources are defined as follows¹⁵:

$$\begin{aligned} \mathcal{O}^a &\equiv i a^6 \sum_{\mathbf{u}, \mathbf{v}} \bar{\xi}(\mathbf{u}) \gamma_5 T^a \xi(\mathbf{v}), \\ \mathcal{O}'^a &\equiv i a^6 \sum_{\mathbf{u}', \mathbf{v}'} \bar{\xi}'(\mathbf{u}') \gamma_5 T^a \xi'(\mathbf{v}'), \end{aligned} \quad (\text{A.9})$$

where ξ and ξ' are the quark fields at the Schrödinger functional boundaries $x_0 = 0$ and $x_0 = T$, respectively.

Appendix B: Properties of $su(N_f)$ Lie algebra generators

Our conventions for the $su(N_f)$ Lie Algebra are those of Appendix A.3. of Ref. [2]. In general, the anti-Hermitian generators of the algebra satisfy

$$[T^a, T^b] = f^{abc} T^c. \quad (\text{B.1})$$

We work in the fundamental representation, with the generators normalised so that

$$\text{Tr}[T^a T^b] = -\frac{1}{2} \delta^{ab}. \quad (\text{B.2})$$

The anticommutator of these generators is given by

$$\{T^a, T^b\} = -i d^{abc} T^c - \frac{\delta^{ab}}{N_f} I_{N_f}, \quad (\text{B.3})$$

where I_{N_f} is the dimension- N_f unit matrix. The structure constants f^{abc} are real and totally antisymmetric tensors, while d^{abc} are real and totally symmetric. Two useful identities are

$$\text{Tr}[T^a T^b T^c] = \frac{1}{4} [i d^{abc} - f^{abc}], \quad (\text{B.4})$$

$$\begin{aligned} \text{Tr}[T^a T^b T^c T^d] &= \frac{1}{4N_f} \delta^{ab} \delta^{cd} \\ &\quad + \frac{1}{8} [d^{abe} + i f^{abe}] [d^{cde} + i f^{cde}] \\ &= \frac{1}{8} \left\{ \frac{2}{N_f} \delta^{ab} \delta^{cd} + d^{abe} d^{cde} - f^{abe} f^{cde} \right. \\ &\quad \left. + i [d^{abe} f^{cde} + d^{cde} f^{abe}] \right\}. \end{aligned} \quad (\text{B.5})$$

For $N_f = 2$ we have $T^a = \tau^a / (2i)$ (τ^a are the Pauli matrices), $f^{abc} = \epsilon^{abc}$ (the Levi-Civita symbol) and $d^{abc} = 0$.

¹⁵ In practice, instead of the sources \mathcal{O}^a and \mathcal{O}'^a defined in Eq. (A.9), we use pseudoscalar smeared sources with wavefunctions at the boundaries, as explained in [29].

For $N_f = 3$ we have $T^a = \lambda^a/(2i)$ (λ^a are the Gell-Mann matrices). The non-vanishing structure constants are

$$\begin{aligned} f^{123} &= 1, \\ f^{147} &= f^{246} = f^{257} = f^{345} = \frac{1}{2}, \\ f^{156} &= f^{367} = -\frac{1}{2}, \\ f^{458} &= f^{678} = \frac{\sqrt{3}}{2}, \end{aligned} \tag{B.6}$$

and their anti-symmetric counterparts. The non-vanishing symmetric constants are

$$\begin{aligned} d^{118} &= d^{228} = d^{338} = \frac{1}{\sqrt{3}}, \\ d^{888} &= -\frac{1}{\sqrt{3}}, \\ d^{448} &= d^{558} = d^{668} = d^{778} = -\frac{1}{2\sqrt{3}}, \\ d^{146} &= d^{157} = d^{256} = d^{344} = d^{355} = \frac{1}{2}, \\ d^{247} &= d^{366} = d^{377} = -\frac{1}{2}, \end{aligned} \tag{B.7}$$

and their symmetric counterparts.

Two useful properties are straightforward consequences of Eqs. (B.6) and (B.7):

- Property A: For any pair of indices a, b , there is at most one value of a third index c for which $d^{abc} \neq 0$.
- Property B: There is no combination of flavour indices a, b, c for which $f^{abc} \neq 0$ and $d^{abc} \neq 0$. In other words, when $f^{abc} \neq 0$, then $d^{abc} = 0$, and when $d^{abc} \neq 0$, then $f^{abc} = 0$.

Appendix C: Renormalisation and improvement

All operators of interest are flavour non-singlets and, unless otherwise stated, quark masses are degenerate. For Wilson fermions, with $O(a)$ Symanzik improvement, we know that the improved current

$$(A_I)_\mu^a = A_\mu^a + a c_A \partial_\mu P^a, \tag{C.1}$$

is correctly normalised a follows:

$$(A_R)_\mu^a = Z_A [1 + b_A am_q + \bar{b}_A a \text{Tr} M_q] (A_I)_\mu^a. \tag{C.2}$$

The renormalised and Symanzik-improved scalar and pseudoscalar densities are given by

$$S_R^a = Z_S [1 + b_S am_q + \bar{b}_S a \text{Tr} M_q] S^a, \tag{C.3}$$

$$P_R^a = Z_P [1 + b_P am_q + \bar{b}_P a \text{Tr} M_q] P^a, \tag{C.4}$$

with $am_q = 1/(2\kappa) - 1/(2\kappa_{\text{crit}})$ the subtracted bare mass; here κ is the Wilson hopping parameter and κ_{crit} its critical value (chiral limit). The mass matrix of subtracted quark masses is denoted by M_q . The current (bare) quark mass, which appears in the chiral Ward identities of the present paper, is defined by the PCAC relation

$$m = \frac{\partial_0 \langle (A_I)_0^a(x) \mathcal{O}^a \rangle}{2 \langle P^a(x) \mathcal{O}^a \rangle}. \tag{C.5}$$

The renormalised quark mass m_R is given in terms of the current mass m by

$$m_R = \frac{Z_A}{Z_P} \frac{[1 + b_A am_q + \bar{b}_A a \text{Tr} M_q]}{[1 + b_P am_q + \bar{b}_P a \text{Tr} M_q]} m. \tag{C.6}$$

For two distinct flavours i, j , the subtracted quark masses are $am_{q,i} = 1/(2\kappa_i) - 1/(2\kappa_{\text{crit}})$ and similarly for $am_{q,j}$. The PCAC mass is defined as

$$m_{ij} = \frac{\partial_0 \langle (A_I)_0^{ij}(x) \mathcal{O}^{ji} \rangle}{2 \langle P^{ij}(x) \mathcal{O}^{ji} \rangle}, \tag{C.7}$$

and the renormalised quark mass average is expressed in terms of m_{ij} as follows:

$$\begin{aligned} \frac{m_{i,R} + m_{j,R}}{2} &= \frac{Z_A}{Z_P} m_{ij} \left[1 + (b_A - b_P) am_{q,ij} \right. \\ &\quad \left. + (\bar{b}_A - \bar{b}_P) a \text{Tr} M_q \right] + O(a^2), \end{aligned} \tag{C.8}$$

where $m_{q,ij} \equiv (m_{q,i} + m_{q,j})/2$. This reduces to Eq. (C.6) for two degenerate masses $m_{q,i} = m_{q,j}$.

In practice for the divergence of the improved axial current we use $\partial_\mu (A_I)_\mu^a \equiv \tilde{\partial}_\mu A_\mu^a + a c_A \partial_\mu^* \partial_\mu P^a$, where $\tilde{\partial}_\mu$ denotes the average of the usual forward and backward derivatives defined as $a \partial_\mu f(x) \equiv f(x + a\hat{\mu}) - f(x)$ and $a \partial_\mu^* f(x) \equiv f(x) - f(x - a\hat{\mu})$.

Appendix D: Charge conjugation, γ_5 -Hermiticity, and correlation functions

Wilson quark propagators in lattices with Schrödinger functional boundary conditions, on a fixed background gauge field, are standard ones, denoted as $[\psi(y) \bar{\psi}(x)]_F$, or boundary-to-bulk ones like $[\zeta(\mathbf{v}) \bar{\psi}(x)]_F$.¹⁶ They all obey the γ_5 -Hermiticity property; e.g.

$$\begin{aligned} [\psi(x) \bar{\psi}(y)]_F^\dagger &= \gamma_5 [\psi(y) \bar{\psi}(x)]_F \gamma_5, \\ [\zeta(\mathbf{v}) \bar{\psi}(x)]_F^\dagger &= \gamma_5 [\psi(x) \bar{\zeta}(\mathbf{v})]_F \gamma_5. \end{aligned} \tag{D.1}$$

¹⁶ See Ref. [28] for their definitions.

Under charge conjugation,¹⁷ the quark bilinear operators of interest transform as follows:

$$\begin{aligned} \bar{\psi}(x)T^a\gamma_5\psi(y) &\rightarrow \bar{\psi}(y)[T^a]^T\gamma_5\psi(x), \\ \bar{\psi}(x)T^a\gamma_0\gamma_5\psi(y) &\rightarrow \bar{\psi}(y)[T^a]^T\gamma_0\gamma_5\psi(x), \end{aligned} \tag{D.2}$$

with $[T^a]^T$ the transpose of $[T^a]$. The time-boundary operators $\bar{\zeta}(\mathbf{u})\gamma_5T^a\zeta(\mathbf{v})$ and $\bar{\zeta}'(\mathbf{u}')\gamma_5T^a\zeta'(\mathbf{v}')$ satisfy analogous properties. Note that in Eqs. (D.1), Wick-contracted fermion fields are same-flavour functions, while in Eqs. (D.2) they are vectors in flavour space.

We now concentrate on the r.h.s. of WI (11), and in particular on Eq. (12) and the traces $F_{S;1}$ and $F_{S;2}$ of Table 1. Using the γ_5 -Hermiticity properties of Eqs. (D.1), it can be easily shown that $F_{S;2}(y_0) = F_{S;1}(y_0)^\dagger$. On the other hand, the traces of three flavour matrices T^{dea} and T^{aed} are given by Eq. (B.4). Putting everything together, the r.h.s. of the Ward identity (11) becomes

$$\begin{aligned} \text{WI r.h.s.} &= -\frac{a^{15}}{2}Z_S d^{bce} \left[d^{ade} \text{Re} \{F_{S;1}(y_0)\} \right. \\ &\quad \left. + i f^{ade} \text{Im} \{F_{S;1}(y_0)\} \right]. \end{aligned} \tag{D.3}$$

Next we apply charge conjugation to the correlation function $\langle \mathcal{O}^a S^e(y) \mathcal{O}^d \rangle$. We see from Eq. (D.2) that the transformation only affects the flavour matrices; instead of $\text{Tr}(T^a T^e T^d)$ we have $\text{Tr}(T^{aT} T^{eT} T^{dT}) = \text{Tr}(T^d T^e T^a)$ and instead of $\text{Tr}(T^d T^e T^a)$ we have $\text{Tr}(T^{dT} T^{eT} T^{aT}) = \text{Tr}(T^a T^e T^d)$. Thus, under a charge conjugation transformation,

$$\begin{aligned} \text{WI r.h.s.} &\rightarrow -\frac{a^{15}}{2}Z_S d^{bce} \left[d^{ade} \text{Re} \{F_{S;1}(y_0)\} \right. \\ &\quad \left. - i f^{ade} \text{Im} \{F_{S;1}(y_0)\} \right]. \end{aligned} \tag{D.4}$$

This should be equal to the original expression (D.3), because charge conjugation leaves QCD correlation functions unaffected. Comparing the last two equations we see that this can only be true if $\text{Im} \{F_{S(1)}(y_0)\}$ vanishes. This proves Eq. (13).

Having shown that the r.h.s. of WI (11) is real, the l.h.s. must also be real. As a crosscheck we show this explicitly. The l.h.s. correlation function is given by Eq. (14), with the traces of flavour matrices given by Eqs. (15)–(20) and the 9 terms $F_{AP;k}$ listed in Table 1. Taking the Hermitean conjugate of these terms we find that the one-boundary ones are related pairwise by complex conjugation,

$$\begin{aligned} T_2^{abcd} F_{AP;2}(x_0, y_0) &= [T_1^{abcd} F_{AP;1}(x_0, y_0)]^*, \\ T_4^{abcd} F_{AP;4}(x_0, y_0) &= [T_3^{abcd} F_{AP;3}(x_0, y_0)]^*, \end{aligned}$$

¹⁷ The Dirac matrix conventions used in the present work are those of Appendix A of Ref. [2]. The charge conjugation conventions are those of Appendix B of the same reference.

$$T_6^{abcd} F_{AP;6}(x_0, y_0) = [T_5^{abcd} F_{AP;5}(x_0, y_0)]^*. \tag{D.5}$$

Hermitean conjugation also implies that the quark-disconnected contributions are real:

$$\begin{aligned} T_7^{abcd} F_{AP;7}(x_0, y_0) &= [T_7^{abcd} F_{AP;7}(x_0, y_0)]^*, \\ T_8^{abcd} F_{AP;8}(x_0, y_0) &= [T_8^{abcd} F_{AP;8}(x_0, y_0)]^*, \\ T_9^{abcd} F_{AP;9}(x_0, y_0) &= [T_9^{abcd} F_{AP;9}(x_0, y_0)]^*. \end{aligned} \tag{D.6}$$

From these properties it immediately follows that the l.h.s. of the WI is real.

However we want to go a step further and show the reality of the traces $F_{AP;1}, \dots, F_{AP;9}$. For the one-boundary contributions, Eqs. (D.5) imply that

$$\begin{aligned} T_1^{abcd} F_{AP;1} + T_2^{abcd} F_{AP;2} &= T_1^{abcd} F_{AP;1} + (T_1^{abcd} F_{AP;1})^* = 2\text{Re} [T_1^{abcd} F_{AP;1}] \\ &= 2[\text{Re} (T_1^{abcd})\text{Re} (F_{AP;1}) - \text{Im} (T_1^{abcd})\text{Im} (F_{AP;1})], \end{aligned} \tag{D.7}$$

with (cf. Eq. (B.5)):

$$\begin{aligned} \text{Re} (T_1^{abcd}) &= \frac{1}{4N_f} \delta^{ab} \delta^{cd} + \frac{1}{8} [d^{abe} d^{cde} - f^{abe} f^{cde}], \\ \text{Im} (T_1^{abcd}) &= \frac{1}{8} [d^{abe} f^{cde} + f^{abe} d^{cde}]. \end{aligned} \tag{D.8}$$

Applying charge conjugation to the 4-point correlation function $\langle \mathcal{O}^a A_0^b(x) P^c(y) \mathcal{O}^d \rangle$, we find that $F_{AP;1} \rightarrow F_{AP;1}$, $F_{AP;2} \rightarrow F_{AP;2}$, and $T_1^{abcd} \leftrightarrow T_2^{abcd}$. Thus under charge conjugation Eq. (D.7) transforms as follows:

$$\begin{aligned} T_1^{abcd} F_{AP;1} + T_2^{abcd} F_{AP;2} &\rightarrow 2[\text{Re} (T_2^{abcd})\text{Re} (F_{AP;1}) - \text{Im} (T_2^{abcd})\text{Im} (F_{AP;1})]. \end{aligned} \tag{D.9}$$

But applying Eq. (B.5) to T_2^{abcd} (cf. also Eq. (D.8)) we see that $\text{Re} (T_2^{abcd}) = \text{Re} (T_1^{abcd})$ and $\text{Im} (T_2^{abcd}) = -\text{Im} (T_1^{abcd})$. Thus, under charge conjugation

$$\begin{aligned} T_1^{abcd} F_{AP;1} + T_2^{abcd} F_{AP;2} &\rightarrow 2[\text{Re} (T_1^{abcd})\text{Re} (F_{AP;1}) + \text{Im} (T_1^{abcd})\text{Im} (F_{AP;1})]. \end{aligned} \tag{D.10}$$

Comparing this result to Eq. (D.7) and recalling that QCD correlation functions remain invariant under charge conjugation, we deduce that $\text{Im} (F_{AP;1}) = 0$. Analogously, $F_{AP;2}, \dots, F_{AP;6}$ are also real. Concerning one-boundary contributions, traces $T_7^{abcd}, T_8^{abcd}, T_9^{abcd}$ are easily seen to be real from Eq. (B.2). The reality of $F_{AP;7}, F_{AP;8}, F_{AP;9}$ then follows immediately from Eqs. (D.6). This completes our proof that also the l.h.s. of WI (11) is real.

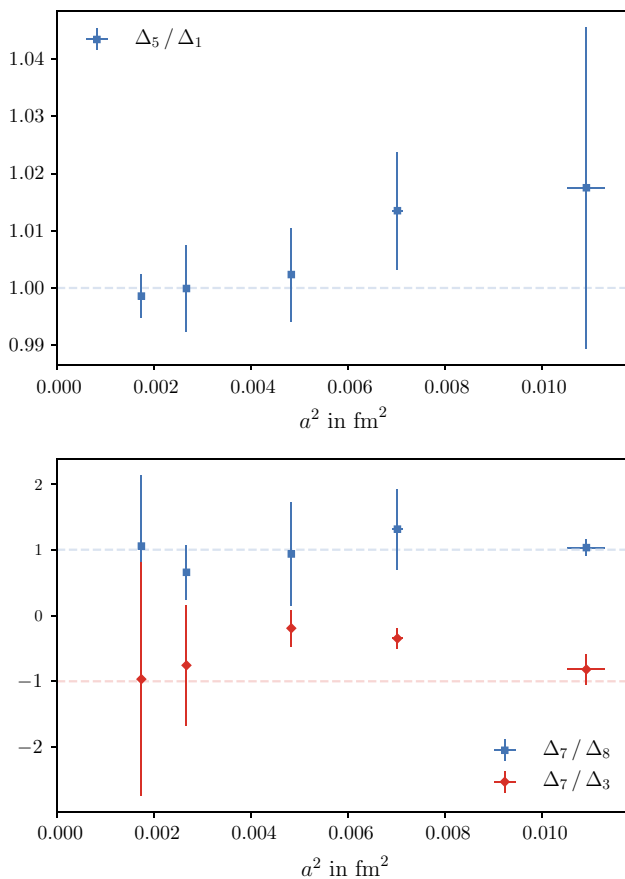


Fig. 8 Non-perturbative confirmation of the identities (24), (27) and (31). In the top panel only quark-connected diagrams contribute to the results, while in the bottom panel quark-disconnected diagrams also give contributions

Appendix E: Non-perturbative checks

As additional validation of our method we want to make sure that the relations (24), (27) and (31) which relate different diagrams to one another are fulfilled up to ambiguities of $O(a^2)$. After making sure that the identities are valid at tree-level of perturbation theory we evaluate them non-perturbatively on our ensembles. The analysis is analogous to the one for the ratio Z_S/Z_P . After evaluating the identities on each lattice for a given value of β , we perform an extra- or interpolation to the chiral point linear in the current quark mass. The values presented here are the results at the chiral point obtained from this procedure. The clearest evidence comes from identity (24) which we can rewrite as

$$\Delta_5 / \Delta_1 = 1 + O(a^2). \tag{E.1}$$

In the top part of Fig. 8 we present the results which show the expected scaling towards the continuum.

The identities (27) and (31) are more complicated to verify as they involve quark disconnected contributions. We can

rewrite the identities as follows

$$\Delta_7 / \Delta_8 = 1 + O(a^2), \tag{E.2}$$

$$\Delta_7 / \Delta_3 = -1 + O(a^2). \tag{E.3}$$

The numerical results are presented in the bottom part of Fig. 8. In this case the statistical uncertainties are orders of magnitudes larger and grow towards the continuum limit. A possible explanation of this is that the Δ_i involved here are vanishing at tree-level in perturbation theory. Despite the large uncertainties our data still suggest that the identities are fulfilled up to the expected ambiguities in the lattice spacing.

References

1. M. Lüscher, Advanced lattice QCD, Proceedings, Summer School in Theoretical Physics, Les Houches. [arXiv: hep-lat/9802029](https://arxiv.org/abs/hep-lat/9802029)
2. M. Lüscher, S. Sint, R. Sommer, P. Weisz, Chiral symmetry and $O(a)$ improvement in lattice QCD. Nucl. Phys. B **478**, 365 (1996). [[arXiv: hep-lat/9605038](https://arxiv.org/abs/hep-lat/9605038)]
3. M. Bochicchio, L. Maiani, G. Martinelli, G.C. Rossi, M. Testa, Chiral Symmetry on the Lattice with Wilson Fermions. Nucl. Phys. B **262**, 331 (1985)
4. A. Vladikas, Three Topics in Renormalization and Improvement, Proceedings, Summer School in Theoretical Physics, Les Houches. [arXiv: 1103.1323](https://arxiv.org/abs/1103.1323)
5. L. Maiani, G. Martinelli, M.L. Paciello, B. Taglienti, Scalar densities and baryon mass differences in lattice QCD with Wilson fermions. Nucl. Phys. B **293**, 420 (1987)
6. G. Martinelli, S. Petrarca, C.T. Sachrajda, A. Vladikas, Nonperturbative renormalization of two quark operators with an improved lattice fermion action. Phys. Lett. B **311**, 241 (1993). [Erratum: Phys. Lett. B **317**, 660 (1993)]
7. G. Martinelli, C. Pittori, C.T. Sachrajda, M. Testa, A. Vladikas, A General method for nonperturbative renormalization of lattice operators. Nucl. Phys. B **445**, 81 (1995). [arXiv: hep-lat/9411010](https://arxiv.org/abs/hep-lat/9411010)
8. J.-R. Cudell, A. Le Yaouanc, C. Pittori, Pseudoscalar vertex, Goldstone boson and quark masses on the lattice. Phys. Lett. B **454**, 105 (1999). [arXiv: hep-lat/9810058](https://arxiv.org/abs/hep-lat/9810058)
9. J.-R. Cudell, A. Le Yaouanc, C. Pittori, Large pion pole in $Z_S^{\text{MOM}}/Z_P^{\text{MOM}}$ from from Wilson action data. Phys. Lett. B **516**, 92 (2001). [arXiv: hep-lat/0101009](https://arxiv.org/abs/hep-lat/0101009)
10. L. Giusti, A. Vladikas, RI / MOM renormalization window and Goldstone pole contamination. Phys. Lett. B **488**, 303 (2000). [arXiv:hep-lat/0005026](https://arxiv.org/abs/hep-lat/0005026)
11. M. Papinutto, New lattice approaches to non-leptonic Kaon decays, Ph.D. thesis (2001)
12. C. Sturm, Y. Aoki, N.H. Christ, T. Izubuchi, C.T.C. Sachrajda, A. Soni, Renormalization of quark bilinear operators in a momentum-subtraction scheme with a nonexceptional subtraction point. Phys. Rev. D **80**, 014501 (2009). [arXiv:0901.2599](https://arxiv.org/abs/0901.2599)
13. M. Lüscher, S. Sint, R. Sommer, H. Wittig, Nonperturbative determination of the axial current normalization constant in $O(a)$ improved lattice QCD. Nucl. Phys. B **491**, 344 (1997). [arXiv:hep-lat/9611015](https://arxiv.org/abs/hep-lat/9611015)
14. M. Della Morte, R. Hoffmann, F. Knechtli, R. Sommer, U. Wolff, Non-perturbative renormalization of the axial current with dynamical Wilson fermions. JHEP **0507**, 007 (2005). [arXiv:hep-lat/0505026](https://arxiv.org/abs/hep-lat/0505026)
15. J. Bulava, M. Della Morte, J. Heitger, C. Wittmeier, Nonperturbative renormalization of the axial current in $N_f = 3$ lattice QCD

- with Wilson fermions and a tree-level improved gauge action. Phys. Rev. D **93**, 114513 (2016). [arXiv:1604.05827](#)
16. S. Sint, The Chirally rotated Schrödinger functional with Wilson fermions and automatic $O(a)$ improvement. Nucl. Phys. B **847**, 491 (2011). [arXiv:1008.4857](#)
 17. M. Dalla Brida, S. Sint, P. Vilaseca, The chirally rotated Schrödinger functional: theoretical expectations and perturbative tests. JHEP **08**, 102 (2016). [arXiv:1603.00046](#)
 18. M. Bruno et al., Simulation of QCD with $N_f = 2 + 1$ flavors of non-perturbatively improved Wilson fermions. JHEP **02**, 043 (2015). [arXiv:1411.3982](#)
 19. M. Bruno, T. Korzec, S. Schaefer, Setting the scale for the CLS $2 + 1$ flavor ensembles. Phys. Rev. D **95**, 074504 (2017). [arXiv:1608.08900](#)
 20. G.S. Bali, E.E. Scholz, J. Simeth, W. Söldner, Lattice simulations with $N_f = 2 + 1$ improved Wilson fermions at a fixed strange quark mass. Phys. Rev. D **94**, 074501 (2016). [arXiv:1606.09039](#)
 21. D. Mohler, S. Schaefer, J. Simeth, CLS $2 + 1$ flavor simulations at physical light- and strange-quark masses. EPJ Web Conf. **175**, 02010 (2018). [arXiv:1712.04884](#)
 22. M. Dalla Brida, T. Korzec, S. Sint, P. Vilaseca, High precision renormalization of the flavour non-singlet Noether currents in lattice QCD with Wilson quarks. Eur. Phys. J. C **79**, 23 (2019). [arXiv:1808.09236](#)
 23. G.M. de Divitiis, P. Fritzsch, J. Heitger, C.C. Köster, S. Kuberski, A. Vladikas, Non-perturbative determination of improvement coefficients b_m and $b_A - b_P$ and normalisation factor $Z_m Z_P / Z_A$ with $N_f = 3$ Wilson fermions. Eur. Phys. J. C **79**, 797 (2019). [arXiv:1906.03445](#)
 24. S. Dürr, Z. Fodor, C. Hoelbling, S. Katz, S. Krieg, T. Kurth et al., Lattice QCD at the physical point: Simulation and analysis details. JHEP **08**, 148 (2011). [arXiv:1011.2711](#)
 25. M. Bruno, I. Campos, P. Fritzsch, J. Koponen, C. Pena, D. Preti et al., Light quark masses in $N_f = 2 + 1$ lattice QCD with Wilson fermions. Eur. Phys. J. C **80**, 169 (2020). [arXiv:1911.08025](#)
 26. J. Heitger, F. Joswig, A. Vladikas, C. Wittemeier, Non-perturbative determination of c_V , Z_V and Z_S/Z_P in $N_f = 3$ lattice QCD. EPJ Web Conf. **175**, 10004 (2018). [arXiv:1711.03924](#)
 27. J. Heitger, F. Joswig, A. Vladikas, Z_S/Z_P from three-flavour lattice QCD. PoS LATTICE2018, 217 (2018). [arXiv:1810.03509](#)
 28. M. Lüscher, P. Weisz, $O(a)$ improvement of the axial current in lattice QCD to one loop order of perturbation theory. Nucl. Phys. B **479**, 429 (1996). [arXiv:hep-lat/9606016](#)
 29. J. Bulava, M. Della Morte, J. Heitger, C. Wittemeier, Non-perturbative improvement of the axial current in $N_f = 3$ lattice QCD with Wilson fermions and tree-level improved gauge action. Nucl. Phys. B **896**, 555 (2015). [arXiv:1502.04999](#)
 30. U. Wolff, Monte Carlo errors with less errors. Comput. Phys. Commun. **156**, 143 (2004). [arXiv:hep-lat/0306017](#). [Erratum: Comput. Phys. Commun. **176**, 383 (2007)]
 31. A. Ramos, Automatic differentiation for error analysis of Monte Carlo data. Comput. Phys. Commun. **238**, 19 (2019). [arXiv:1809.01289](#)
 32. P. Fritzsch, J. Heitger, N. Tantalo, Non-perturbative improvement of quark mass renormalization in two-flavour lattice QCD. JHEP **08**, 074 (2010). [arXiv:1004.3978](#)
 33. J. Heitger, F. Joswig, The renormalized $O(a)$ improved vector current in three-flavour lattice QCD with Wilson quarks, in preparation
 34. P. Fritzsch, A. Ramos, F. Stollenwerk, Critical slowing down and the gradient flow coupling in the Schrödinger functional. PoS Lattice **2013**, 461 (2014). [arXiv:1311.7304](#)
 35. S. Schaefer, R. Sommer, F. Vrotta, Critical slowing down and error analysis in lattice QCD simulations. Nucl. Phys. B **845**, 93 (2011). [arXiv:1009.5228](#)
 36. P. T. Boggs, J. E. Rogers, Orthogonal distance regression, tech. rep., National Institute of Standards and Technology, Gaithersburg, MD (1989). <https://doi.org/10.6028/NIST.IR.89-4197>
 37. M. Constantinou, V. Lubicz, H. Panagopoulos, F. Stylianou, $O(a^2)$ corrections to the one-loop propagator and bilinears of clover fermions with Symanzik improved gluons. JHEP **10**, 064 (2009). [arXiv:0907.0381](#)
 38. J. Garden, J. Heitger, R. Sommer, H. Wittig, Precision computation of the strange quark's mass in quenched QCD. Nucl. Phys. B **571**, 237 (2000). [arXiv:hep-lat/9906013](#)
 39. P. Fritzsch, F. Knechtli, B. Leder, M. Marinkovic, S. Schaefer, R. Sommer et al., The strange quark mass and Lambda parameter of two flavor QCD. Nucl. Phys. B **865**, 397 (2012). [arXiv:1205.5380](#)
 40. J. Heitger, G.M. von Hippel, S. Schaefer, F. Vrotta, Charm quark mass and D-meson decay constants from two-flavour lattice QCD. PoS LATTICE2013, 475 (2014). [arXiv:1312.7693](#)
 41. J. Heitger, F. Joswig, S. Kuberski, Towards the determination of the charm quark mass on $N_f = 2 + 1$ CLS ensembles. PoS LATTICE2019, 092 (2019). [arXiv:1909.05328](#)
 42. I. Campos, P. Fritzsch, C. Pena, D. Preti, A. Ramos, A. Vladikas, Non-perturbative quark mass renormalisation and running in $N_f = 3$ QCD. Eur. Phys. J. C **78**, 387 (2018). [arXiv:1802.05243](#)
 43. T. Bhattacharya, R. Gupta, W. Lee, S.R. Sharpe, J.M. Wu, Improved bilinears in lattice QCD with non-degenerate quarks. Phys. Rev. D **73**, 034504 (2006). [arXiv:hep-lat/0511014](#)
 44. S. Capitani, M. Lüscher, R. Sommer, H. Wittig, Non-perturbative quark mass renormalization in quenched lattice QCD. Nucl. Phys. B **544**, 669 (1999). [arXiv:hep-lat/9810063](#). [Erratum: Nucl. Phys. B **582**, 762 (2000)]
 45. M. Constantinou, M. Hadjiantonis, H. Panagopoulos, Renormalization of flavor singlet and nonsinglet fermion bilinear operators. PoS LATTICE2014, 298 (2014). [arXiv:1411.6990](#)
 46. P. Korcyl, G.S. Bali, Non-perturbative determination of improvement coefficients using coordinate space correlators in $N_f = 2 + 1$ lattice QCD. Phys. Rev. D **95**, 014505 (2017). [arXiv:1607.07090](#)
 47. J. Bulava, S. Schaefer, Improvement of $N_f = 3$ lattice QCD with Wilson fermions and tree-level improved gauge action. Nucl. Phys. B **874**, 188 (2013). [arXiv:1304.7093](#)